REVIEW

Chang'e-5 lunar samples shed new light on the Moon

Yi Chen,[1,7] Sen Hu,[2,7] Jin-Hua Li,[2,7] Qiu-Li Li,[1,7] Xiongyao Li,[3,7] Yang Li,[3,7] Yang Liu,[4,7] Yuqi Qian,[5,7] Wei Yang,[2,7] Qin Zhou,[6,7] Yangting Lin,[2,*] Chunlai Li,[6,*] and Xian-Hua Li[1,*]

*Correspondence: linyt@mail.iggcas.ac.cn (Y.L.); licl@nao.cas.cn (C.L.); lixh@gig.ac.cn (X.-H.L.)

Received: May 20, 2023; Accepted: June 22, 2023; Published Online: June 23, 2023; https://doi.org/10.59717/j.xinn-geo.2023.100014

GRAPHICAL ABSTRACT

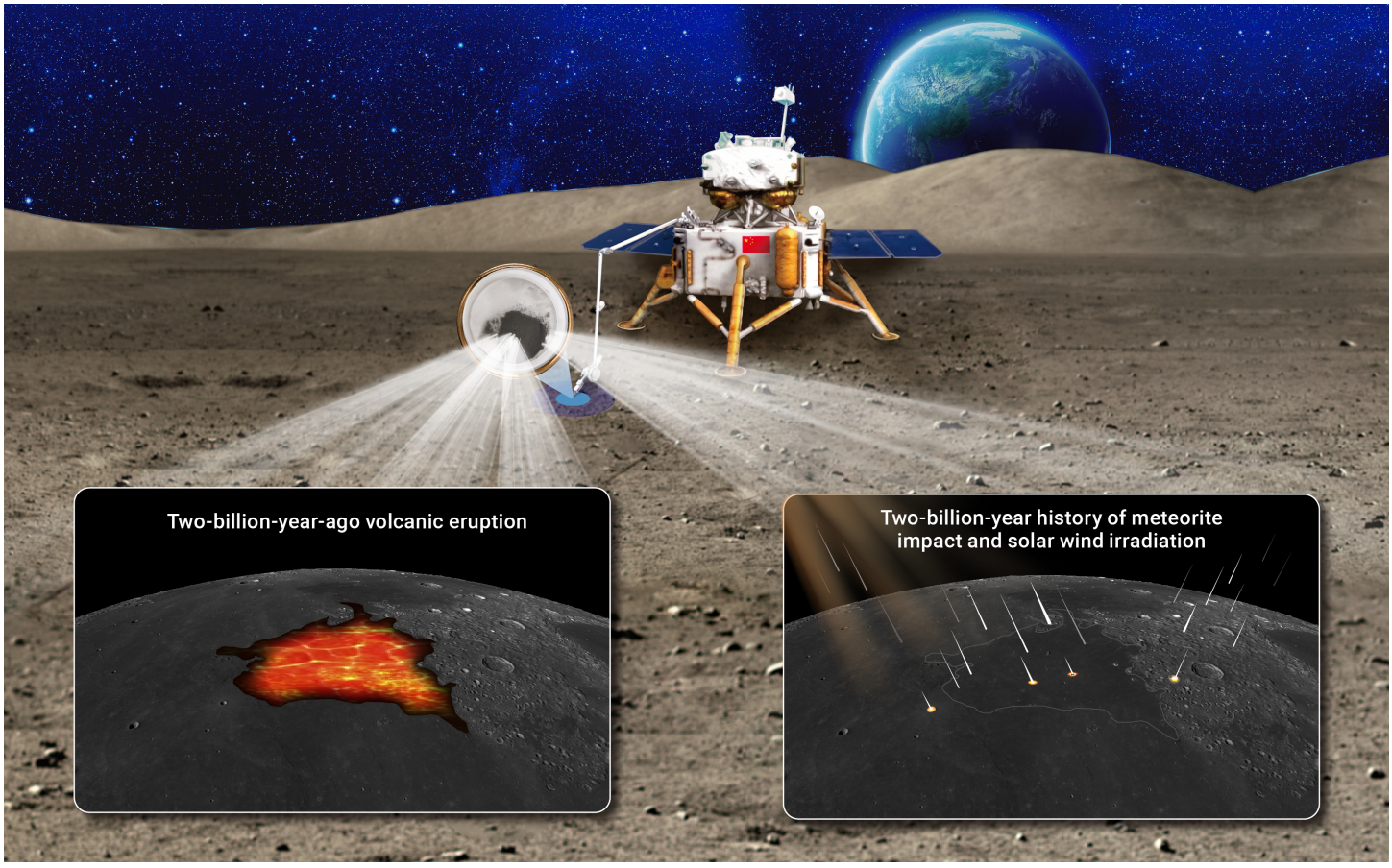

PUBLIC SUMMARY

- This overview summarizes the main findings from the new lunar soil samples collected by the Chang'e-5 mission.
- The soil is mature, which contains basalt and mineral fragments, impact melt breccia, agglutinates, and glasses.
- Analysis of basalt fragments reveals that the Moon was still volcanically active two billion years ago.
- The soil, dominated by local materials, provides a unique example to study meteorite impact and solar wind irradiation.

REVIEW

www.the-innovation.org/geoscience

Chang'e-5 lunar samples shed new light on the Moon

Yi Chen,[1,7] Sen Hu,[2,7] Jin-Hua Li,[2,7] Qiu-Li Li,[1,7] Xiongyao Li,[3,7] Yang Li,[3,7] Yang Liu,[4,7] Yuqi Qian,[5,7] Wei Yang,[2,7] Qin Zhou,[6,7] Yangting Lin,[2,*] Chunlai Li,[6,*] and Xian-Hua Li[1,*]

[1]State Key Laboratory of Lithospheric Evolution, Institute of Geology and Geophysics, Chinese Academy of Sciences, Beijing 100029, China
[2]Key Laboratory of Earth and Planetary Physics, Institute of Geology and Geophysics, Chinese Academy of Sciences, Beijing 100029, China
[3]Center for Lunar and Planetary Sciences, Institute of Geochemistry, Chinese Academy of Sciences, Guiyang 550081, China
[4]State Key Laboratory of Space Weather, National Space Science Center, Chinese Academy of Sciences, Beijing 100190, China
[5]State Key Laboratory of Geological Processes and Mineral Resources, School of Earth Sciences, China University of Geosciences, Wuhan 430074, China
[6]Key Laboratory of Lunar and Deep Space Exploration, National Astronomical Observatories, Chinese Academy of Sciences, Beijing 100101, China
[7]These authors contributed equally
*Correspondence: linyt@mail.iggcas.ac.cn (Y.L.); licl@nao.cas.cn (C.L.); lixh@gig.ac.cn (X.-H.L.)

Received: May 20, 2023; Accepted: June 22, 2023; Published Online: June 23, 2023; https://doi.org/10.59717/j.xinn-geo.2023.100014

Citation: Chen Y., Hu S., Li J., et al., (2023). Chang'e-5 lunar samples shed new light on the Moon. The Innovation Geoscience 1(1), 100014.

The Chang'e-5 (CE-5) mission, the first return of lunar samples to Earth since the Apollo and Luna missions more than 44 years ago, landed on one of the youngest mare basalt units (1.0-3.0 Ga, based on superposed crater counts), located at middle latitude (~43°N) far from previous landing sites. On December 17, 2020, the sample capsule returned to Earth with 1731 grams of lunar soil collected from the upper few centimeters of the surface and from an ~1 meter-long core drilled into the lunar regolith. This paper summarizes the main discoveries of the CE-5 samples allocated since July 12, 2021, and measured with state-of-the-art analytical techniques. Physical property studies indicate that the CE-5 soil is mature, with a peak particle size of ~50 μm (in volume), and a particle size distribution similar to the sub-mature and mature Apollo lunar soils (<1 cm). The soil sample contains basalt and mineral fragments, impact melt breccia, agglutinates, and glasses. The basalt fragments can be divided into several petrographic types, likely crystallized from the same lava flow at different depths and cooling rates. The CE-5 basalt Pb/Pb SIMS analyses yielded a crystallization age of 2.030 ± 0.004 Ga, extending the duration of lunar volcanic activity by ~1.0~0.8 Ga. This age, in turn, has helped to calibrate the widely applied lunar crater chronology model. The isotopic ratios of Pb, Nd and Sr indicate that the contribution of a KREEP component in forming CE-5 basalt is limited (<0.5%), excluding high concentrations of heat-producing radioactive elements in their mantle source. The isotope analyses of H, Cl, and S reveal that the mantle source is dry, which cannot account for the prolonged volcanism observed in the CE-5 landing region. A possible explanation is that the CE-5 mantle source contains enhanced clinopyroxene-ilmenite cumulate (~20%), which reduces the melting temperature by ~80°C. The REE-, FeO-enrichment of the CE-5 basalt can be attributed to a low degree of partial melting followed by extensive fractional crystallization. The CE-5 soil has also recorded a two-billion-year history of meteorite impact and solar wind irradiation. A few exotic fragments have been recognized (some with high-pressure silica phases) and are likely ejected from distant lunar highlands. The U-Pb dating of impact glass beads reveals at least 17 main impact events. New space weathering effects, especially the formation of Fe^{3+}, have been found. *In situ* reflectance spectra and laboratory analyses of CE-5 soil show the presence of water (in the form of H, OH, and/or H_2O). The solar wind hydrogen was implanted and concentrated in the outermost rims (<100 nm) of soil grains, with a temperature (hence latitude)-dependent maximum water concentration of up to ~2 wt%.

INTRODUCTION

Geological samples are crucial to revealing the origin and evolution of a planet. Our current knowledge of the Moon comes primarily from the nine Apollo and Luna sample return missions' landing sites (the 1960s and 1970s), lunar meteorites, and orbital remote sensing data. However, the Apollo and Luna sample sites only represent a limited area on the nearside, close to the equator. They are clearly not representative of the entire history of lunar volcanism (Figure 1).[1,2] For example, mare basalts with intermediate TiO_2 contents are rare in the Apollo and Luna sample collections,[3] and relatively young volcanic rocks were never returned.[4] Many critical questions remain to be answered by more diverse sample collection strategies,[5] but until the Chang'e-5 (CE-5) mission, new samples had not been returned since the Luna 24 mission in 1976.

To enhance our knowledge of the late-stage evolution of the Moon, China undertook the CE-5 sample-return mission, targeted to a young unsampled mare unit. CE-5 launched on November 24, 2020, landed on the lunar surface on December 1, 2020, and returned to the Earth on December 17, 2020,[6,7] with 1,731 grams of collected samples.[8] The CE-5 landing/sampling site is located in Northern Oceanus Procellarum (43.06°N, 51.92°W;[7] Figure 1A-B) on an Eratosthenian-aged, intermediate-Ti, smooth mare plain termed Em4/P58 (4th Eratosthenian-aged mare unit in the region;[9] 58th mare unit in Oceanus Procellarum).[10] The Em4/P58 unit is ~40-50 m thick,[11,12] and overlies older Imbrian-aged, low-Ti mare basalts. Crater size-frequency distribution (CSFD) measurements indicated that this unit had an absolute model age (AMA) between 1.2-3.0 Ga.[10,12–15]

The new CE-5 lunar samples can help investigate and answer many fundamental questions about lunar evolution. For example, what is the absolute age of the Em4/P58 unit, and how can this age improve the precision of the lunar crater counting chronology in the inner Solar System? What is the leading mechanism that triggered this late-stage lunar volcanism? What is the contribution of KREEP in forming the CE-5 basalts? What is the estimated volatile content of the CE-5 basalts? Were the glasses in the CE-5 soil produced by impact processes or explosive volcanism? How do they relate to the petrology and age of the CE-5 basalt if they were volcanic? Can they reveal the impact flux at the landing area if they were impact in origin? Are any exotic non-mare materials in the CE-5 soil? If so, what are their provenances and ages? What is the difference between space weathering in mid-latitude and low-latitude? How much can solar wind hydrogen be implanted and retained in the CE-5 soil?

Since the first allocation of the CE-5 samples on July 12, 2021, Chinese scientists have conducted systematic studies to address these issues. A series of original and fundamental achievements have been reported in the physical properties and chemical composition of the CE-5 soil,[8,16–20] the age and nature of late lunar volcanic activity,[21–33] the age and composition of impact glasses,[34–36] lunar surface space weathering[37-43] and micro-analytical technologies.[44–46] Given that the CE-5 samples will soon be allocated to international scientists, this paper aims to synthesize the recent studies in the CE-5 samples to maximize the scientific findings of the new samples and promote international collaboration in the future.

BULK SOIL

Physical properties

The Ground Research and Application System (GRAS, https://Moon.bao.ac.cn/web/enmanager/home) first undertook a comprehensive preliminary analysis of the characteristics of the CE-5 samples, which provided basic physical and chemical information for sample allocation and further investigation.[8] The reported major physical parameters are summarized in Figure 2, including particle size distribution, density, and specific surface area (SSA).[8,19]

Particle size distribution is a fundamental physical parameter that affects the strength, compressibility, and optical and thermal properties of lunar soil. The particle size of the CE-5 soil is concentrated around 50 μm (median grain

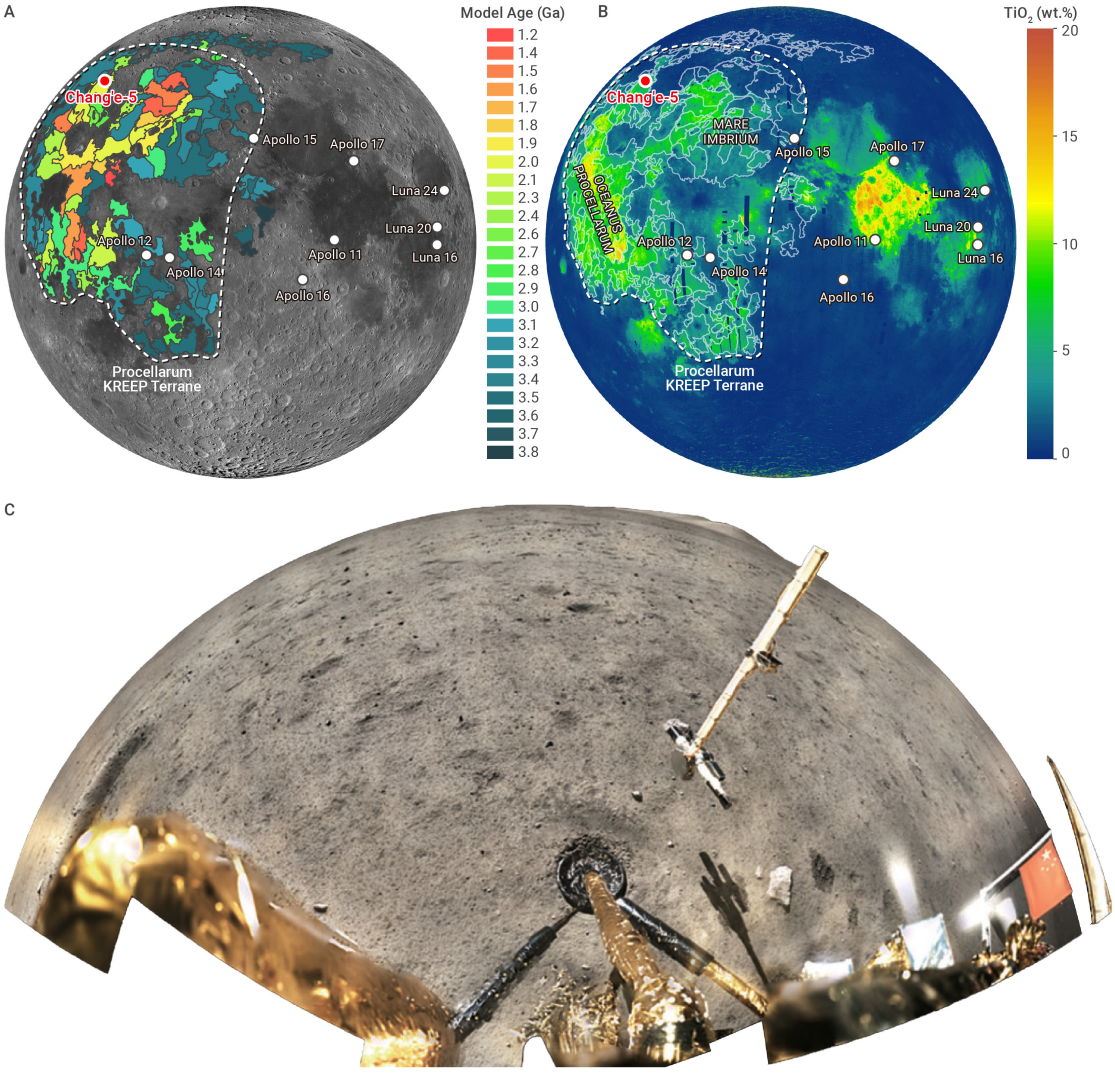

Figure 1. The CE-5 landing site and scooped sampling on the Moon (A) Model ages of mare basalts in the Procellarum KREEP Terrane, with landing sites of CE-5, Apollo and Luna sample return missions indicated. Data are from Qian et al. (2023).[28] (B) TiO_2 contents of mare basalts in Procellarum KREEP Terrane. Data are from Lucey et al. (2000).[47] (C) A partial image of CE-5 scooped sampling (after Li C. et al. 2022[8]).

size) with a single peak in their particle size-mass (volume) distribution, similar to the sub-mature and mature lunar soils of the Apollo missions.[49] In addition, the number and modal mass distributions and the coefficients of uniformity and curvature indicate that CE-5 lunar soil is well-graded and sorted.[8,19] Therefore, the CE-5 sample has been classified as mature lunar soil based on its particle size distribution.[8] It should be noted that the large fragments exceeding 0.5 cm in CE-5 lunar soils were manually picked out during sample processing. The remaining lunar soils were then subject to particle size analysis.

The density contributes to understanding the composition, elasticity, thermal diffusivity, porosity, and compressibility of lunar soils.[50] The true density (without considering the volume of pores) of the CE-5 soil (3.20 g/cm^3) is close to Apollo 11 and Apollo 15 lunar soils (3.24 g/cm^3) but higher than that of Apollo 12 and Apollo 14 (~2.9 g/cm^3). This high density may be related to the high FeO and TiO_2 contents of CE-5 lunar soil. Although the bulk composition of the CE-5 soil indicates that it is mainly sourced from local mare basalt,[20] the true density of CE-5 soil is slightly lower than that of lunar basalt (3.25-3.57 g/cm^3).[48]

The SSA related to the adsorption and surface activity of lunar particles also reflects the size and irregular shape of the particles.[51] The measured SSA of CE-5 soil (0.56 m^2/g) is within the range of the Apollo samples (0.02-0.78 m^2/g),[48] indicating a relatively constant particle size and shape of lunar soils globally.[48,52] Due to the small SSA values, water molecules are difficult to retain either in Apollo or CE-5 soil grains.[53]

In situ and laboratory spectroscopic studies

The lunar surface "ground truth" is crucial for interpreting orbital spectral data. *In situ* and laboratory spectral analyses of the lunar samples serve as critical validations of remote sensing observations. For instance, it was speculated that the composition of the late-stage, intermediate-Ti basalts in Oceanus Procellarum was olivine-rich, based on orbital observations displaying a broad 1 μm spectral feature.[54] To test this idea, Liu et al. (2022) performed laboratory spectral analyses of returned CE-5 samples and the results show that the diagnostic spectral features are attributed to the high abundance of iron-rich, high-Ca pyroxenes (HCP) rather than olivine.[27] The possible misinterpretation of the orbital remote sensing was attributed to the mixing effect and spectral similarities between iron-rich HCP and olivine, especially at short wavelengths. These laboratory spectral results shed light on understanding the mineralogy of other highly evolved (hence FeO-enriched) young basalts in the Procellarum KREEP Terrane.[27]

In addition, the photometric properties of the lunar regolith play critical roles in interpreting orbital spectral data. Using the *in situ* data from the Lunar Mineralogical Spectrometer (LMS) onboard the CE-5 lander,[55] Xu J. et al. (2022)[56] derived the photometric parameters of the regolith at the sampling site, and they found that backward scattering was negligible and forward scattering was dominant in the CE-5 sampling zone. These parameters can

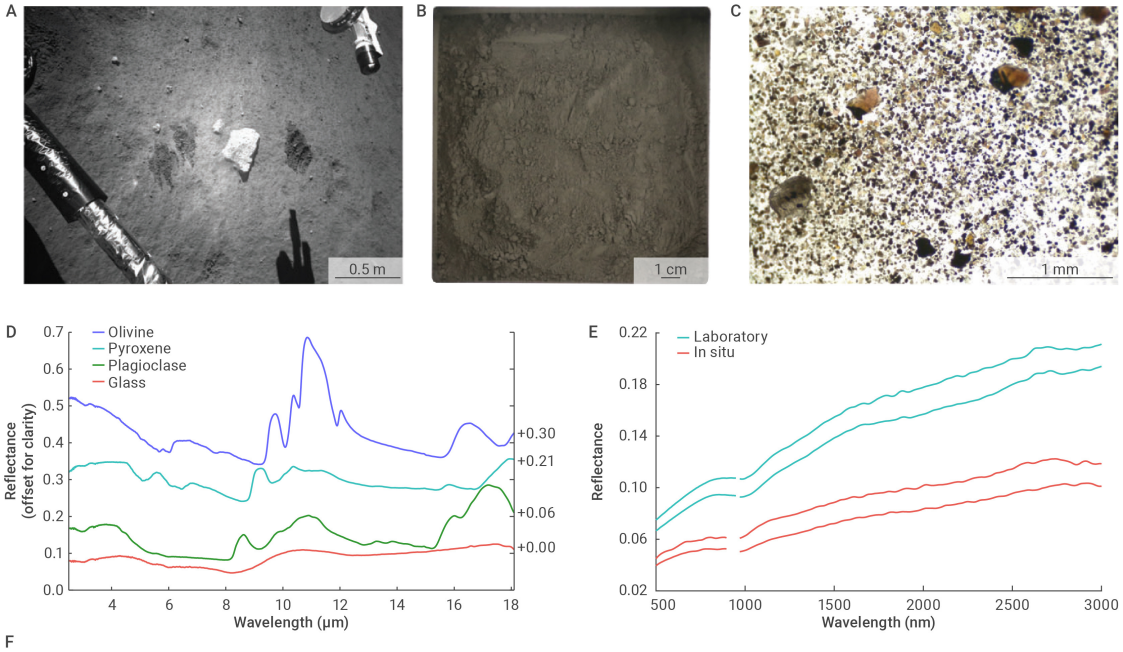

F

Physical parameter	CE-5 lunar soil	Apollo lunar soils
Equivalent diameter	1.40~ 9.35 μm (mean 3.96 μm, 95% in number) 4.84~432.27 μm (mean 49.80 μm, 95% in mass)	24 ~ 429 μm (range of means from 307 samples, sieving measurement)
Median grain size	52.54~55.24 μm	28 ~ 493 μm (range of medians from 307 samples, sieving measurement)
Modal mass	0.0036~0.8304 ng (mean 0.5567 ng)	––
Circularity	0.875	––
Bulk density	1.24 g/cm^3	––
True density	3.20 g/cm^3	2.9~3.44
Specific surface area	0.56 m^2/g	0.02~0.78

Figure 2. Photos, spectra, and physical properties of the CE-5 soil (A) Monitoring camera photo of the CE-5 sampling site. The sample was mostly gray-black. The dark traces are the imprints after sampling. (B) Photo of the CE-5 soil sample in the laboratory. (C) Microscope photo of CE-5 soil particles (e.g., yellow-green olivine, white feldspar, brown-black pyroxene, and brown glass). (D) Laboratory spectra of the major phases from the CE-5 soil. (E) Comparison of the *in situ* and laboratory spectra of the CE-5 soil. (F) Basic physical properties of the CE-5 soil compared with the Apollo soil samples. Data are from refs.[8,19,48,49]

serve as ground truth, which can then be used in radiative transfer modeling analysis of orbital remote-sensing data to derive mineral abundances. Yang Y. et al. (2022)[57] measured the micro mid-infrared reflectance spectra of individual CE-5 soil grains in the laboratory, including typical lunar minerals (olivine, pyroxene, and plagioclase) and glass samples, and derived their optical constants. These optical properties build a link between the returned sample and orbital spectral data, which can be used to determine the best-fit composition that corresponds to the spectrum of a remotely observed surface.

Spectroscopy is also widely used to evaluate the optical maturity and model the nanoscale metallic iron (Fe^0) particle content of lunar regolith.[58–60] Using the *in situ* spectral measurements from LMS, Wu et al. (2022)[61] estimated the optical maturity and Fe^0 content of the CE-5 sampling site. The results show no obvious variations between undisturbed and disturbed (by the descent stage of CE-5) regions, suggesting that the disturbance from rocket exhaust did not affect the measured regolith maturity. Additionally, the surficial regolith, and the scooped underlying layer at the centimeter-depth at the CE-5 landing area, exhibit similar maturities, suggesting rapid gardening.[62] Lu et al. (2023)[63] derived Fe^0 content using both the *in situ* and the lab-measured visible and near-infrared reflectance spectra with the returned samples. Large Fe^0 particles (micron-size) were also found in the sample, which likely formed as relict meteoritic Fe-Ni metal fragments and/or dense clustering of oversaturated Fe^0 in FeO-rich basalts.[63]

Except for changing the optical maturity of lunar soils, space weathering, such as solar wind implantation, can contribute to the accumulation of lunar surficial water. LMS onboard CE-5 covers the water absorption wavelengths around 2.85 μm and provides the first opportunity for *in-situ* investigation of the water content on the Moon using reflectance spectroscopy.[64] After thermal correction using an empirical model,[65,66] the *in situ* spectra at the CE-5 sampling site show apparent water absorptions. Detailed analyses show that the lunar regolith at the sampling site contains water content up to ~120 ppm, mostly attributed to solar wind implantation.[64] The presence of the solar-wind implanted water was subsequently confirmed by the analysis of CE-5 mineral grains with the micron FTIR[43] and nano-SIMS[42] techniques in the laboratory. The cross-comparison between the *in situ* and laboratory analyses reinforces the robustness of spectroscopy in estimating water content on the Moon.

Petrography

In a manner similar to the Apollo lunar soils,[67] the CE-5 lunar soil is also comprised of different components, including mineral and lithic fragments, glasses, and agglutinates (Figure 3A-D).[8,22,31]

Approximately 45~53% of lithic fragments are basalt.[31,68] The basalt fragments in the CE-5 lunar soil show poikilitic, subophilitic, porphyritic, or equigranular textures (Figure 3E-H). They are composed of clinopyroxene, plagioclase, olivine, and ilmenite, with minor Cr-spinel, troilite, and mesostasis, including K-feldspar, silica, fayalite, phosphates, and Zr-rich phases.[8,21,25,26,29,31]

The breccias mainly consist of mineral and lithic clasts, vesicle-rich impact melts, and agglutinates, with a few fragments containing high silicic clasts and exotic materials.[69–71] The mineral clasts mainly include plagioclase, pyroxene, olivine, and ilmenite, whereas the lithic clasts are almost exclu-

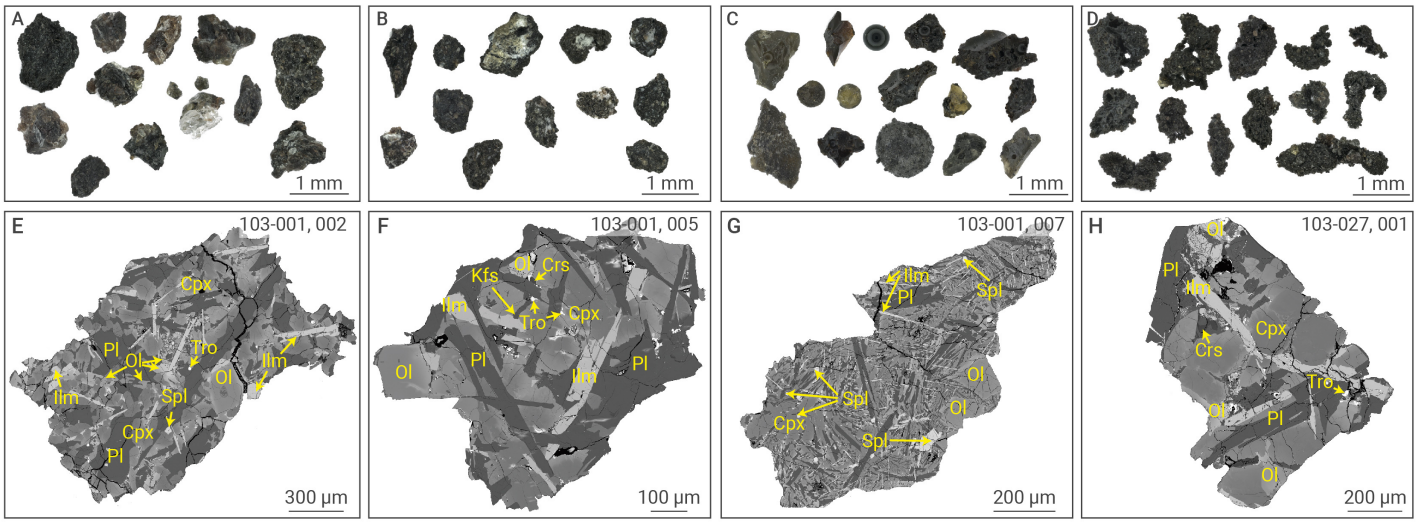

Figure 3. Microscope photos and Back-scatter electron (BSE) images of the particles in the CE-5 soil (A-D) Microscope photos of basalt fragments, breccia, glasses and agglutinates (after Yang W. et al., 2022[68]). (E-H) BSE images of four representative types of basalt fragments: poikilitic, subophitic, porphyritic, and equigranular (after Tian et al. 2021[31]).

sively basalt. The surfaces of clasts are occasionally covered by variable amounts of glass.[8]

On the basis of their morphological differences, glassy materials in lunar soils are divided into two principal categories.[8] One is round glass beads, variable in color, mostly black and brown, with occasional green glass beads. The other is irregularly shaped glass fragments with obvious shell-like fractures. Brown pits are sometimes visible on the glass surface. They are texturally dominated by clast-rich and homogeneous particles, with a small amount being quench crystallized.[34,36]

Agglutinates comprise lithic and mineral fragments welded together by the glass produced by melting due to micrometeoroid impacts. Agglutinates are irregular in shape, loose and easily broken, with relatively well-developed pores.

The proportions of these four constituents in CE-5 soil have yet to be reported. According to Yang et al. (2022),[68] 146 particles larger than 355 μm, including 40 basalt, 36 breccia, 37 agglutinate, 32 glass, and 1 olivine fragments, were picked from a 1.5 g CE-5 soil sample. However, these proportions may not represent the bulk soil, as the finer fraction contains higher proportions of mineral fragments and glasses, similar to Apollo and Luna samples.[67] In addition, the X-ray diffraction and Raman analyses of the bulk soil exhibit a range of variability, indicating 26.4 to 39.4 % plagioclase, 31.6 to 42.0 % pyroxene, 5.7 to 9.8 % olivine, 1.9 to 6.0 % ilmenite, 8.0 to 24.4 % glass and agglutinate in the CE-5 soil.[8,16] However, all reported major and trace element compositions of the bulk soil are consistent (Table 1).

BASALT FRAGMENTS

Many studies have been conducted on basalt fragments from the CE-5 soil.[21-23, 25, 26, 29-33, 72, 73] Here, we compile the available compositional data of 73 basalt fragments (Table 1) with individual fragments ranging from 200 to 2000 μm.

Chemical and mineral compositions

The CE-5 basalt fragments have lower clinopyroxene (30.9-49.5%) but higher plagioclase abundances (29.3-47.4%)[28,29,31] relative to Apollo basalts (clinopyroxene: 47.7-68.4%; plagioclase:19.2-41.2%).[74] No orthopyroxene has been reported in the CE-5 basalt fragments. Clinopyroxene has a wide compositional range ($En_{0.6\text{-}47.7}Wo_{11.8\text{-}41.7}$) with Mg-Ca-rich cores and Fe-rich, Ca-poor rims (Figure 4A).[25,31,32] It shows variable, parallel REE patterns with negative Eu anomalies,[30,31] indicative of evolving compositional variation during crystallization.

Plagioclase is anorthite-rich ($An_{60\text{-}94}$, Figure 4B, except for minor mesostasis grains being albite-rich) and has variable TiO_2 contents (0.03-0.84 wt%).[21,30,31] The grains commonly have Ca-Mg-rich, K-poor cores relative to the rims,[32] reflecting the depletion of Ca and Mg in the residual melt. They show variable but parallel rare-earth element (REE) patterns with positive Eu anomalies, and have homogeneous and low initial $^{87}Sr/^{86}Sr$ ratios (0.69934-0.69986).[30,31] These results indicate that the plagioclase grains crystallized at different stages from a single lava flow.[31]

Olivine occurs as phenocrysts, anhedral inclusions in plagioclase, subhedral-anhedral grains coexisting with clinopyroxene, or anhedral mesostasis phases.[31,33] The olivine phenocrysts and inclusions have Mg-rich cores ($Fo_{60\text{-}61}$),[22,25,31] indicating an early crystallization phase. The mesostasis olivine is Fe-rich (Fo<15) and thus represents a late-stage phase. Titanium contents in olivine range from 409 to 2603 ppm, initially increasing and then decreasing with the reduction of Fo values (Figure 4C).[33] This feature indicates that the evolving magma changed from ilmenite undersaturated to saturated, similar to the evolution trend of low-Ti basalt. The parental magma has ~4.4 wt% TiO_2 as estimated by the most primitive olivine (Fo_{60}),[33] slightly higher than that (~3.5 wt%) displayed by the primitive plagioclase (An_{90}),[30] but still within the low-Ti basalt range.

Ilmenite mainly occurs as fine-grained, orientated lamellae crosscutting Mg-rich olivine phenocrysts (Fo>50),[25,29,31] consistent with a crystallization phase later than olivine. However, ilmenite also shows coarse-grained phases in equilibrium with low-Mg olivine (Fo<44).[21] These textures reflect ilmenite solidification during the middle stage of fractional crystallization, which is a typical characteristic of low-Ti basalt.[75] The MgO content in ilmenite (<2.32 wt%)[22,25,31] is lower than that of Apollo low-Ti (<5.2 wt%) and high-Ti basalts (<9.1wt%),[76] indicative of crystallization from Mg-poor magma.

The bulk major-element compositions of the CE-5 basalt fragments have been constrained using the modal recombination method,[21,31] laser ablation inductively coupled plasma mass spectrometry (LA-ICP-MS),[22] or standard-based energy dispersive (EDS) X-ray mapping.[29,73] All these approaches yield scattered bulk compositions (Figure 4D). Compared to Apollo and Luna basalts, the CE-5 basalts have lower MgO (4.87 wt% on average) and higher FeO (22.1 wt% on average) contents, likely due to higher crystallization degrees or different primary magma compositions.

Lunar mare basalts are classified primarily based on their bulk TiO_2 contents.[74] The low-Ti basalt (1.0 wt% < TiO_2 < 6.0 wt%) and high-Ti basalt (TiO_2 > 6.0 wt%) represent two distinct evolutionary trends of Ti-undersaturated and Ti-saturated magmas, respectively. However, the TiO_2 contents of the CE-5 basalt fragments are variable (3.0 to 16.3 wt%), making it difficult to identify their affinity. The scattered TiO_2 contents may be caused by (1) unrepresentative sampling due to small fragment size or limited grains, (2) large uncertainties of the modal recombination method, or (3) evolving TiO_2 contents in the parental magma during crystallization. Choosing large fragments (> 500 μm) with abundant, homogeneously distributed mineral

Table 1. Chemical compositions of the CE-5 soil, basalt fragments and glasses

Ref.	CE-5 soil[8,20]			CE-5 basalt fragments[22,29,31,72,73]						CE-5 glasses[34–36]			
	[Li]	[Zong]	This study[a]	[Tian]	[Su]	[He]	[Yuan]	[Jiang]	This study[a]	Mid-Ti	Low-Ti	High-Al	High-Mg
(%)	**n=2**	**n=7**	**n=9**	**n=13**	**n=27**	**n=8**	**n=23**	**n=2**	**n=73**	**n=147**	**n=4**	**n=7**	**n=3**
SiO_2	42.2	41.3	41.5	42.1	42.0	43.7	44.6	41.9	43.0	40.2	44.4	49.3	48.7
TiO_2	5.00	5.12	5.09	5.7	5.5	4.06	5.7	5.75	5.45	5.47	2.28	2.03	2.27
Al_2O_3	10.8	11.6	11.4	11.6	13.2	10.0	10.4	9.68	11.6	12.3	11.8	16.4	7.35
Cr_2O_3				0.2	0.2		0.1	0.21	0.16	0.17	0.23	0.20	
FeO	22.5	22.7	22.7	22.2	22.1	21.9	21.9	24.7	22.1	21.9	18.8	11.1	11.2
MnO	0.28	0.28	0.28	0.3	0.3	0.29	0.2	0.30	0.27	0.26	0.24	0.15	0.33
MgO	6.48	6.25	6.30	5.8	4.4	5.54	4.6	5.63	4.87	7.22	10.9	8.5	21.3
CaO	11.0	11.6	11.5	10.9	11.2	12.5	11.6	10.9	11.4	11.9	10.9	11.0	7.6
Na_2O	0.26	0.46	0.42	0.6	0.8	0.5	0.2	0.47	0.53	0.07	0.05	0.32	0.33
K_2O	0.19	0.21	0.21	0.1	0.2	0.22	0.1	0.22	0.15	0.03	0.01	0.19	0.07
P_2P_5	0.23	0.27	0.26	0.2		0.32	0.3	0.29	0.27	0.03	0.02	0.04	0.01
Total	98.9	99.7	99.6	99.7	99.9	99.0	99.7	100.1	99.8	99.5	99.7	99.3	99.2
Mg#	34.1	33.1	33.4	32.0	26.4	31.1	27.4	29.1	28.4	37.3	51.2	58.0	77.3
(μg/g)	**n=2**	**n=7**	**n=7**			**n=9**		**n=2**	**n=2**	**n=40**	**n=2**	**n=2**	
Li		15.4	15.4			15.5		14.8	14.8	11.0	10.0	30.6	
B										1.70	3.70	2.25	
Be		2.84	2.84					2.7	2.7				
Sc	66	62.9	62.9			78.6		62.9	62.9	61.1	44.5	31.1	
V	95.8	92.5	92.5			78.6		88.9	88.9	79.4	94.0	43.0	
Cr	1410	1459	1459			921		1405	1405	1153	1561	1363	
Co	40	37.2	37.2			29.4		32.4	32.4	34.9	29.4	12.2	
Ni	136	139	139			37.1		18.6	18.6	81.2	21.6	14.6	
Cu		12.2	12.2					15.3	15.3	0.28	0.08	0.34	
Zn	16.2	14.2	14.2					9.7	9.7	1.98	0.29	1.00	
Ga		5.79	5.79					6.0	6.0	3.45	2.31	6.69	
Ge													
Rb	7.47	5.23	5.23			5.59		4.9	4.9	0.47	0.20	2.81	
Sr	276	313	313			332		351	351	326	138	201	
Y		116	116			109		115	115	106	78	302	
Zr	458	545	545			450		571	571	546	295	1464	
Nb		35.6	35.6			26.9		36.3	36.3	35.5	16.5	82.5	
Mo		0.03	0.03										
Cs	0.17	0.22	0.22			0.25		0.21	0.21	0.03	0.02	0.07	
Ba	362	395	395			423		409	409	418	177	979	
La	36.1	35.4	35.4	37.5		36.4		37.2	37.2	37.3	19.9	96.8	
Ce	92.8	98.6	98.6	105		96.2		103	103	90.2	48.4	233	
Pr	12.5	12.7	12.7			12.4		13.4	13.4	13.1	7.16	32.4	
Nd	58.4	59.3	59.3	66.0		57.5		61.4	61.4	60.8	34.8	153	
Sm	16.1	17.0	17.0	18.2		17.7		17.8	17.8	17.6	9.74	43.4	
Eu	2.56	2.77	2.77	1.2		2.79		3.0	3.0	2.79	1.43	2.90	
Gd	18.9	19.6	19.6	19.2		19.4		19.8	19.8	20.0	12.2	49.5	
Tb	3.51	3.27	3.27	3.0		3.37		3.3	3.3	3.28	2.12	8.80	
Dy	20.9	20.5	20.5	19.6		22.8		20.6	20.6	21.7	14.7	58.5	
Ho	4.5	4.07	4.07			4.15		4.1	4.1	4.29	3.12	12.3	
Er		11.3	11.3	10.4		13.0		11.2	11.2	11.9	8.64	33.9	
Tm	0.80	1.57	1.57			1.79		1.5	1.5	1.58	1.18	4.87	
Yb	9.49	9.9	9.9	9.2		11.2		9.3	9.3	9.89	7.61	29.5	
Lu	1.41	1.36	1.36	1.3		1.48		1.3	1.3	1.40	1.19	4.22	
Hf	13.6	14.0	14.0			12.9		14.5	14.5	15.1	7.99	36.3	
Ta	1.77	1.83	1.83			1.46		1.8	1.8	1.82	0.80	3.54	
W		0.50	0.50										
Pb		1.89	1.89					1.6	1.6	0.08	0.02	0.02	
Th	4.72	5.14	5.14	4.5		4.68		5.1	5.1	5.49	2.92	18.1	
U	1.41	1.35	1.35			1.43		1.3	1.3	0.91	0.41	3.42	

[a] This study recommends average compositions of CE-5 bulk soil and basalt. The major elements are calculated by averaging all available data, while the trace elements are cited from ICP-MS data by Zong et al. (2022)[20] and Jiang et al. (2023)[72] for CE-5 bulk soil and basalt, respectively. The trace element compositions obtained by different studies are consistent, but the ICP-MS technique provides relatively more accurate results and allows for analyses of more elements.

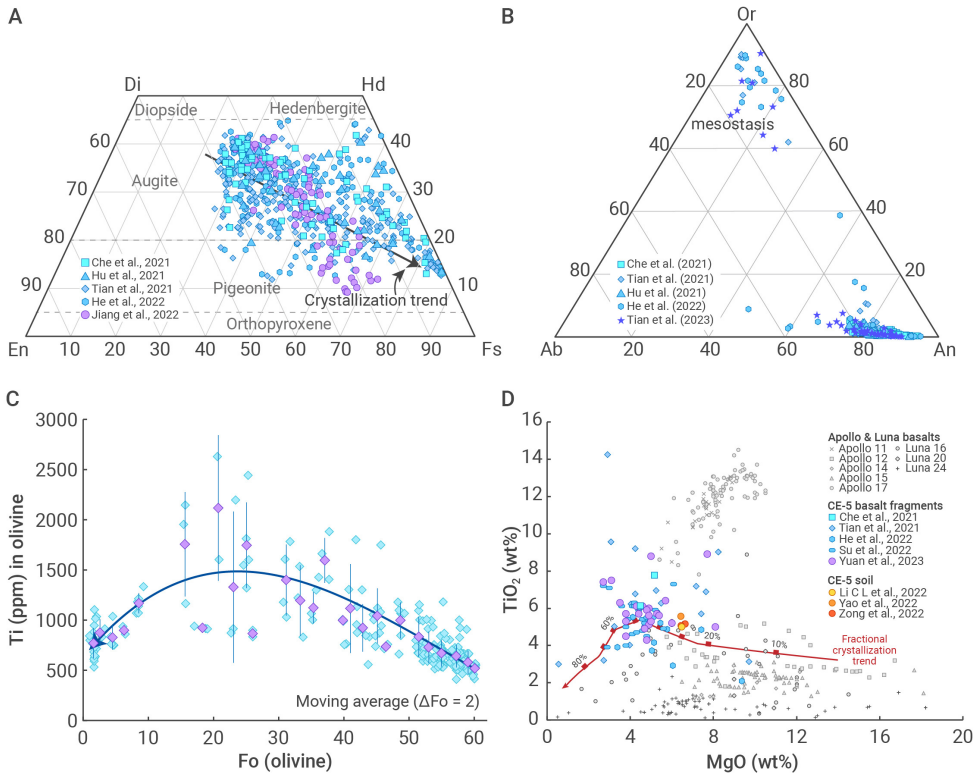

Figure 4. Mineral and whole-rock chemistry of the CE-5 basalt fragments (A) Quadrilateral diagram of pyroxene in the CE-5 basalt. (B) Ternary diagram of plagioclase content in the CE-5 basalt. (C) Ti versus Fo of olivine in the CE-5 basalt. Blue diamonds are plots for Ti and Fo values of olivine. Purple diamonds with vertical error bars (1SD) represent average Ti contents calculated for ΔFo = 2 intervals. The blue curve with an arrow represents the best fit to the average results. (D) TiO_2 versus MgO (wt%) in CE-5 basalts and soils, and Apollo and Luna basalts. The Apollo and Luna data are from Clive Neal's Mare Basalt Database (https://www3.nd.edu/~cneal/Lunar-L/). The CE-5 basalt data are taken from Che et al. (2021),[21] Tian et al. (2021),[31] He et al. (2022),[22] Su et al. (2022),[29] and Yuan et al. (2023).[73] The soil sample data are collected from Li C. et al. (2022),[8] Yao et al. (2022),[18] and Zong et al. (2022).[20] The red line is taken from forward fractional crystallization modeling (1 kbar) based on the reserved primary magma for the CE-5 basalts.[29]

grains would yield more accurate results.[29,73] Overall, the majority of the basalt fragments (>80%) are chemically clustered at 3.8-6.2 wt% TiO_2 and 3.5-6.0 wt% MgO (Figure 4D), corresponding to ~40-70% fractional crystallization from the CE-5 primary magma.[29] In addition, olivine and plagioclase chemistry, as well as petrological modeling, indicate that the TiO_2 content of the parental magma would first increase and then decrease during crystallization.[29,30,33] This evolution trend is similar to the Apollo low-Ti basalt but distinct from the Apollo high-Ti basalt (Figure 4D). Some Ti-rich basalt fragments (TiO_2>6.0 wt%)[21,25] may represent products during the middle crystallization stage, as also evidenced by olivine in these fragments being Fe-rich (Fo_{19-44}).

Isotopic ages

Precise and accurate isotopic dating of the CE-5 basalt is essential to determine the timing of magmatic activity in the landing area and to calibrate the crater-counting results. The Zr-bearing minerals (baddeleyite, zirconolite and tranquillityite) are ideal for dating due to U enrichment, with negligible non-radiogenic Pb. However, these minerals are generally <3~8 μm in size, which is challenging for precise dating. Two research teams independently conducted *in-situ* SIMS Pb-Pb dating on the CE-5 basalts. The team led by the Institute of Geology, Chinese Academy of Geological Sciences employed SHRIMP Pb isotope analyses on 50 selected spots within phosphate grains, K-feldspar grains, K-rich glass pockets and areas containing Zr-rich minerals of two basalt fragments, with spot diameters of about 7 μm. A Pb-Pb isochron approach was adopted to yield 1963 ± 57 Ma, which is interpreted as the age of the basalt (Figure 5A).[21] Another team led by the Institute of Geology and Geophysics, Chinese Academy of Sciences, applied SIMS Pb/Pb dating techniques on all four types of basalt fragments, including 17 poikilitic, 18 subophitic, 10 equigranular and 2 porphyritic fragments. A ~3 μm spot size was fine-tuned to provide additional accuracy by avoiding terrestrial, laboratory-derived Pb contamination along grain boundaries and lunar non-radiogenic Pb of the surrounding silicates. Four isochrons were constructed to yield ages of 2027 ± 7 Ma, 2030 ± 6 Ma, 2034 ± 8 Ma and 2027 ± 54 Ma for the poikilitic, subophitic, equigranular and porphyritic fragments, respectively. Despite the distinct petrographic textures in CE-5 basalts, these four isochrons show consistent ages and slopes, indicating their near-simultaneous formation and derivation from the same source. A total of 159 analyses, including the fifty-one grains of Zr-rich minerals, yielded a precise age of 2030±4 Ma (Figure 5A), considered the best estimate of the crystallization age of the CE-5 basalts.[26] The radiometric methods provide conclusive evidence that magmatic activity on the Moon persisted until at least 2 Ga ago. Furthermore, the age of CE-5 basalt provides a critical reference point to bridge the unanchored middle portion of the lunar crater counting chronology (Figure 5B), improving the dating accuracy of unsampled surfaces on the Moon as well as the other inner Solar System bodies such as the Mars.[77,78]

Petrogenesis and mantle sources

The petrogenesis of CE-5 basalt is crucial to understanding the source and nature of the young volcanic activity[12] and the thermo-chemical evolution of the Moon.[75] Although the reported basalt fragments exhibit various textures and mineral modes, they all originated from the same basalt magma and have similar mineral chemistry. For example, all analyzed clinopyroxene grains follow the same trends in Ti/(Ti + Cr) vs. Mg# and Ti vs. Al diagrams,[36] suggesting that they crystallized from the same magma.[80] The average major and trace element compositions of basalt estimated from basalt fragments,[22,29,31] bulk soil[20] and impact glasses[36] are consistent, which supports the in-depth discussion of the origin and source characteristics of the CE-5 basalts. These studies agree that CE-5 basalt represents a highly evolved volcanic rock with low Mg# values and high FeO contents.[20,22,29,31,36] Olivine and plagioclase chemistry and petrological modeling suggest that the parental magma is Ti-undersaturated, similar to the Apollo low-Ti basalt.

The contribution of the KREEP component in forming the CE-5 basalt is a major key to understanding the mechanism producing young volcanism on the Moon. Young mare basalts distributed within Procellarum KREEP Terrane were thought to be formed from KREEP-rich sources at depth.[81] The CE-5 basalt has ~4.5 ppm Th and is enriched in rare earth elements (REE) and incompatible trace elements, higher than the Apollo low-Ti basalts.[20,22,31] It exhibits enriched light rare earth elements (LREE), and the REE pattern looks very similar to that of KREEP basalt.[31,36] However, there are some differences in the REE patterns between the CE-5 basalt and KREEP. The CE-5 basalt has a smaller Eu anomaly with $(Eu/Eu^*)_N \approx 0.45$ and higher LREE/HREE ratios (e.g., La/Yb ≈ 3.71).[36] These characteristics cannot be reproduced by mixing with KREEP.[36] In addition, the initial Sr-Nd-Pb isotopic compositions of the CE-5 basalt are inconsistent with the origin of KREEP-rich source materials.[21,26,31]

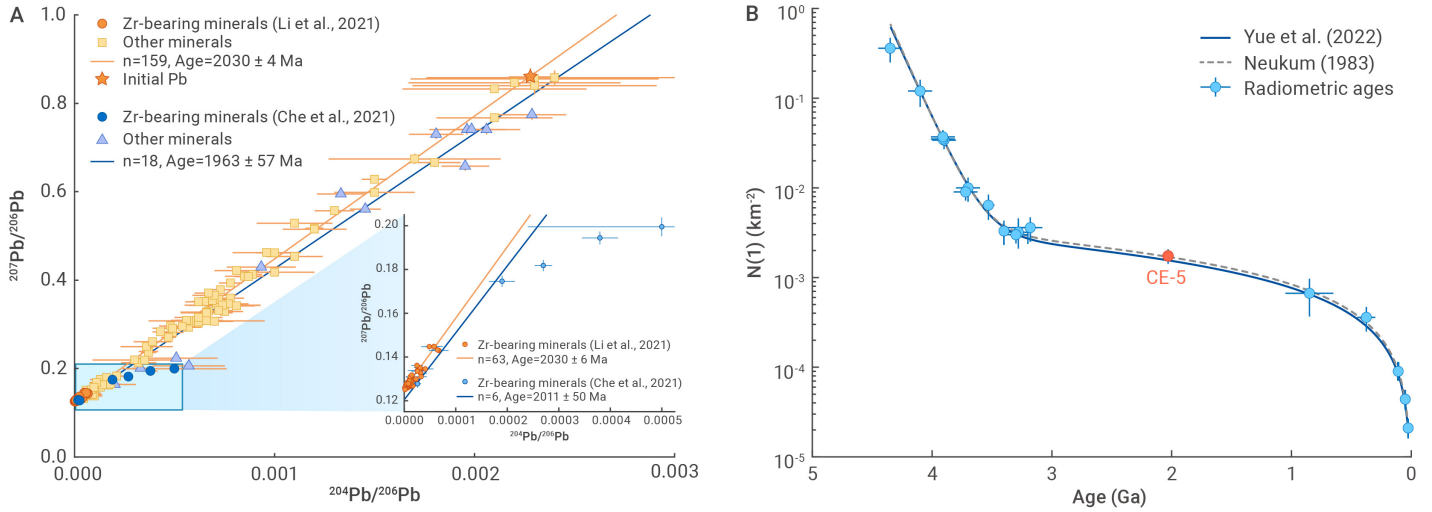

Figure 5. Age of the CE-5 basalt and calibration of the lunar crater chronology model (A) Pb/Pb isochrons of CE-5 basalt fragments. Data are from Li Q. et al. (2021)[26] and Che et al. (2021).[21] (B) New lunar chronology model[78] and comparison with the widely used Neukum's model.[79]

Based on their $^{147}Sm/^{144}Nd \approx 0.222–0.227$ and $^{87}Rb/^{86}Sr \approx 0.009–0.022$, the contribution of KREEP in the mantle source of the CE-5 basalt is estimated to be < 0.3-0.5%[31] or 1-1.5%.[20] These different estimations mainly come from the proposed mineral modes of the mantle source. Tian et al. (2021)[31] and Yang W. et al. (2022)[36] followed the model of Snyder et al. (1992),[82] which is widely used to estimate the contribution of KREEP materials in the Apollo samples and lunar meteorites.[83] Zong et al. (2022)[20] proposed a new model, adding 40-60% REE-depleted clinopyroxene into the mantle source to make it possible to contain more REE-enriched KREEP-rich materials. Luo et al. (2023) combined quantitative textural analyses of the CE-5 basalt, diffusion chronometry, clinopyroxene geothermobarometers and crystallization simulations to determine the pressure and temperature of the mantle source, which they calculated to be 0-13 kbar and 1350±50°C.[84] They suggested that the source is likely to be an olivine-bearing pyroxenite, but did not provide any supporting evidence for this hypothesis. In contrast, Su et al. (2022)[29] conducted fractional crystallization and mantle melting simulations. The results indicate that the mantle source of the CE-5 basalt contains only 20% clinopyroxene-ilmenite (Cpx-Ilm) cumulates. Jiang et al. (2023)[72] suggested that approximately 20-30% of clinopyroxene-ilmenite cumulates in the mantle source of the CE-5 basalt based on its Mg-Fe isotopic compositions. Despite these differences, it is clear that the contribution of KREEP materials in forming the CE-5 basalt is quite limited. To explain the LREE enrichment of the CE-5 basalt, extensive (43–78%) fractional crystallization after low-degree (2–3%) melting was proposed,[31,85] which is also consistent with the low Mg# and high FeO signatures of CE-5 basalt. Thermophysical modeling based on clinopyroxene Mg-Fe zoning of CE-5 basalt suggested that the thickness[32] of the lava flow was at least 21-118 m with a volume of 777-3626 km^3. The extensive fractional crystallization implies that there should be a region of vast underplating (e.g., networks of sills, dikes, and magma chambers) of 3,530~16,480 km^3 or greater. Therefore, although the overall lunar volcanic activity decreases over time, magmatic flux was enhanced at about 2.0 Ga.

Fractional crystallization and mantle melting simulations for the CE-5 basalt and the Apollo low-Ti basalts also show that the Apollo low-Ti basalts may be derived from a source containing (90%) Ol + Opx and (10%) Cpx + Ilm, while the CE-5 basalt appears to be derived from a source containing (80%) Ol + Opx and (20%) Cpx + Ilm.[29] In other words, the CE-5 mantle source included more clinopyroxene-ilmenite cumulates than the sources of Apollo low-Ti basalts. These late-stage fusible cumulates of the lunar magma ocean can lower the melting point of the mantle by ~80°C, triggering this young mare volcanism.[29] The geochemical characteristics of the CE-5 basalt and its origin are summarized in Figure 6.

Water and volatiles

To constrain the water abundance for the mantle source of the CE-5 mare basalt, Hu S. et al. (2021)[23] measured the water abundance and hydrogen isotopes of apatite and ilmenite-hosted melt inclusions from 23 basalt fragments in two CE-5 soil sample aliquots using nano-SIMS. Euhedral apatite occurs mainly in mesostasis of the CE-5 mare basalt fragments with a modal abundance of less than 0.4 vol%, indicating that it was a very late crystallization mineral. The majority of CE-5 apatite contains water abundances ranging from 555 ± 31 to 4856 ± 217 ppm (avg. = 1921 ± 910 ppm, 1SD) with δD values ranging from 275 ± 85‰ to 1022 ± 87‰ (avg. = 578 ± 208‰, 1SD), comparable with those reported in high-Ti and low-Ti Apollo basalts. The ilmenite-hosted melt inclusions contain water abundances from 6 ± 2 ppm to 370 ± 21 ppm and show a wide range of δD values from -330 ± 190‰ to 869 ± 230‰. The negative correlations between the water abundances and δD values of ilmenite-hosted melt inclusions reflect H_2 degassing during the progressive evolution of the parent magma. The CE-5 apatite crystallized later than the melt inclusions display a D-enriched feature (δD > 275‰), consistent with the crystallization sequence of the parent magma of CE-5 mare basalts.[22,31]

Therefore, the water (283 ± 22 ppm) measured in the most D-depleted melt inclusions probably represented the water content of the parent magma, consistent with the estimate (600 ± 400 ppm) using apatite. Considering a low degree partial melting (2-3%) of the mantle source and a moderate to high degree fractional crystallization (43-78%) of the parent magma,[31] a maximum water abundance for the mantle source of CE-5 basalts is estimated to be 1-5 ppm. This value is notable in that it is at the lower end of the mantle water abundance range derived from other lunar samples. It excludes the possibility that a high water abundance in the lunar mantle reservoir could be a major cause of the prolonged volcanic activity of CE-5 mare basalts by reducing the melting temperature of the lunar mantle source.[23]

Furthermore, other volatiles (e.g., S and Cl) play a geochemical role similar to water in magmatic processes.[86] Liu X.Y. et al. (2022)[87] performed detailed petrographic, mineral chemistry, and in situ sulfur isotope analysis on sulfides from the CE-5 basalts. A bulk sulfur abundance of 360 ± 180 ppm for the CE-5 basalts was estimated according to the modal abundance and mineral chemistry of sulfides. Meanwhile, a decreasing trend of $\delta^{34}S$ in the parent magma with crystallization and degassing was observed in CE-5 sulfides, indicating that 40% S was lost during the eruption and crystallization of the parent magma, and the parent magma of the CE-5 basalts could have a sulfur content of 600 ± 300 ppm. The estimated sulfur abundance in the mantle source is 1-10 ppm, which suggests sulfur depletion in the CE-5 mantle source.

Chlorine isotope compositions of lunar samples display the widest variation among solar system objects (e.g., refs.[88,89]). Ji et al. (2022)[24] performed systematic petrography, mineral chemistry, volatile abundances, and Cl isotope studies on the apatite from CE-5 basalts to investigate chlorine isotope characteristics and fractionation mechanisms for lunar volcanism.

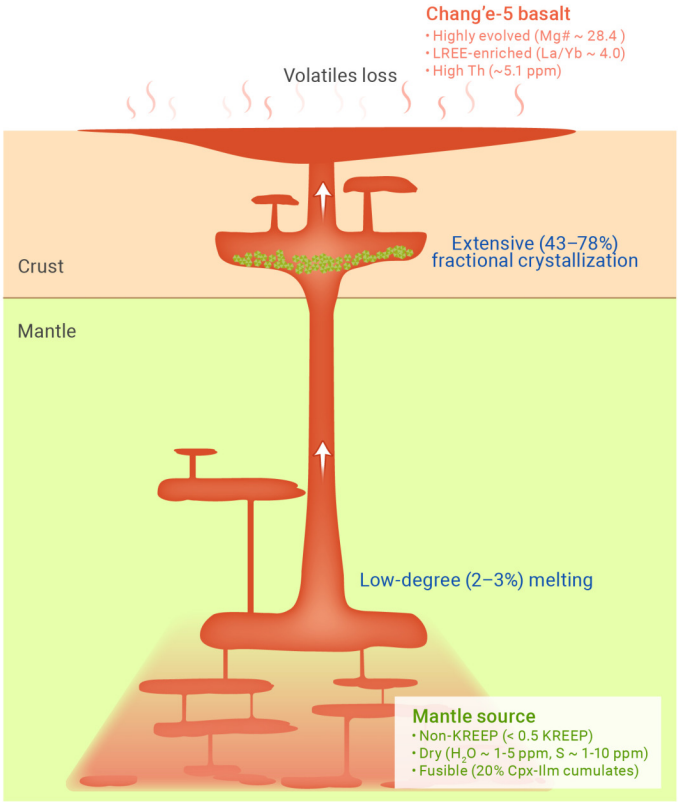

Figure 6. Interpretive diagram showing the geochemical characteristics of the CE-5 basalt and its origin.

Chlorine displays notable zoning distributions in some CE-5 apatite grains with higher abundance at the rims, gradually decreasing towards the cores. The $\delta^{37}Cl$ values of CE-5 apatite vary from 4.5 to 18.9‰, positively correlated with the Cl abundances (820 to 11989 ppm), and this positive correlation was even notable within individual basalt fragments. As apatite is a late crystallization mineral and the Cl content of apatite is an arbitrary index to reflect its crystallization sequence,[90,91] the positive correlation between Cl abundances and $\delta^{37}Cl$ values, Cl zoning signature, and petrographic textures of the CE-5 apatite suggest that magmatic degassing of Cl-bearing species during the crystallization of apatite on or near the lunar surface could have resulted in an extensive Cl isotope fractionation, highlighting a significant role of magmatic fractionation of Cl isotopes during crystallization of mare lavas.

Although both water and sulfur are depleted in the mantle source of CE-5 basalts, their abundances in the parent magma are comparable with the estimates from Apollo basalts.[92] The high abundances of the volatiles in the magma of CE-5 basalt were due to concentrating processes, i.e., low degree partial melting of the mantle source followed by high degree fractional crystallization.[23,24,31] The CE-5 finally basalt became dry due to the persistent degassing loss of volatiles during the eruption and crystallization on the lunar surface.

IMPACT GLASSES

The glasses in the CE-5 lunar soil contain round glass beads and irregularly shaped glass fragments. Analysis of 615 glass beads, including their microstructure, petrology, geochemistry and chronology, with diameters ranging from approximately 20 to 300 μm have been reported.[34–36]

Both impacts and volcanic eruptions can form the glass beads found in lunar soils (e.g., refs.[93–95]). Therefore, the first issue that needs to be addressed is the origin of the CE-5 glass beads. On the basis of BSE images, three major varieties of texture were recognized: (1) clast fragment-bearing microbreccia, (2) quench crystallized glass, and (3) clean glass (Figure 7A-C). Approximately 72.9% of glass beads are clast fragment-bearing microbreccia, indicating an impact origin.[34–36] The other two types are also considered to be impact glasses because (1) most of them (e.g., 89.6% of clean glass) have similar compositions to that of the CE-5 lunar soil (Figure 7D-E),[34–36] (2) their refractory elements (TiO_2, Al_2O_3, MgO and CaO) exhibit negative correlations with SiO_2, while the volatile elements (Na_2O, K_2O and P_2O_5) positively correlate with SiO_2, indicating vaporization of SiO_2.[36] The vaporization loss of SiO_2 has never been reported in any volcanic glass but was previously observed in the Al-rich impact glasses from the Apollo 16 soils;[94,96] (3) the ages of the glasses are all younger than the CE-5 basalt (Figure 7F).[34]

Through chemical and chronological studies of the impact glasses in the Apollo and Luna soils, valuable insights have been gained regarding their provenances of origin and the timing of the Moon's impact flux.[94,95,97–103] Therefore, the ages and chemical compositions of CE-5 glass beads can also serve as indicators of their provenances and short-term variations of the impact flux.

Based on the chemical composition of the 164 clean glasses reported by three studies,[34–36] at least four chemical groups can be recognized: (1) mid-Ti basaltic, (2) low-Ti basaltic, (3) high-Al and (4) high-Mg (Figure 7D). The mid-Ti basaltic group is dominant, accounting for 147 of the 164 glasses. They form a loose compositional cluster for major and trace elements, which is similar to the CE-5 bulk soil on average (Figure 7D-E). These results indicate that local materials dominate the source of CE-5 impact glasses and are consistent with the study of the bulk chemical composition of the CE-5 soil which suggested that exotic materials are less than 5 wt.%.[20] Other glasses, low-Ti basaltic, high-Al and high-Mg, exhibit major and trace elements distinct from that of the CE-5 soil, indicating exotic sources. For example, the high-Al glasses show similar trace element compositions as those in KREEP basalt, and are likely to have been delivered from Aristarchus crater.[36] The low-Ti glasses might have been ejected from the P10 mare unit located northwest of the landing site or the material underneath the CE-5 basalt layer.[36]

Long et al. (2022)[34] reported the first batches of SHRIMP U-Pb dating results on 215 impact glasses in the CE-5 soil. They found that those clast-bearing and incompletely homogenized particles tend to contain greater proportions of older inherited Pb. The impact glass beads representing the local chemical group have formation ages ranging from a few million years to 2 Ga. Applying an "unmixing" approach, they identified 17 statistical groups. Compared with the CSFD within the landing site, the potential source craters that contributed impact glasses to the soil sample collected by the CE-5 were evaluated. Notably, there are a few consistent ages between lunar impact glasses and terrestrial impact craters, suggesting the potential co-evolution history of meteorite impacts in the Moon-Earth system. However, the age populations of impact glasses in the CE-5 soil are not entirely consistent with those of Apollo impact glasses. Specifically, the CE-5 impact glasses do not exhibit the same ~800 and ~500 Ma impact spikes, as well as the increased impact rate in the past ~290 Ma observed in Apollo impact glasses.[101] The cause of this inconsistency remains unclear. More studies are still required to distinguish Moon-wide events.

EXOTIC COMPONENTS

According to studies on the bulk CE-5 soil and impact glasses, the amount of exotic materials in the soil is relatively low, accounting for less than 5%.[20,36] The CE-5 soil stands out from other landing sites, as it is predominantly sourced from a single basalt unit, which is remarkably distinct from the Apollo or Lunar soil samples.[20]

The CE-5 bulk soils have slightly higher MgO (6.48-7.07 wt%; Figure 4D) and Ni (130-167 ppm) contents[8,18,20] relative to the basalt fragments (4.87 wt% MgO and 18.6 ppm Ni in average).[22] Studies on the Apollo and Luna samples revealed that the elevated Ni concentrations in lunar soils could be attributed to the presence of meteoritic materials.[106,107] Similarly, Zong et al. (2022)[20] estimated that the CE-5 soil is comprised of approximately 1 wt% of meteoritic materials. The slightly higher MgO contents in bulk soils relative to the basalt fragments may suggest the presence of some Mg-rich materials, such as exotic Mg-rich glasses[34] and lithic fragments of olivine pyroxenite, magnesian anorthosite, troctolite, and other Mg-suite rocks.[69,71]

By investigating CE-5 samples, a wide range of exotic components has been recognized, e.g., igneous clasts, impact ejecta and glasses.[34–36,69,71,108,109] The igneous clasts include fragments of high-Ti vitrophyric, low-Ti basalt, olivine-pyroxenite, magnesian anorthosite, an evolved lithology, Mg-rich

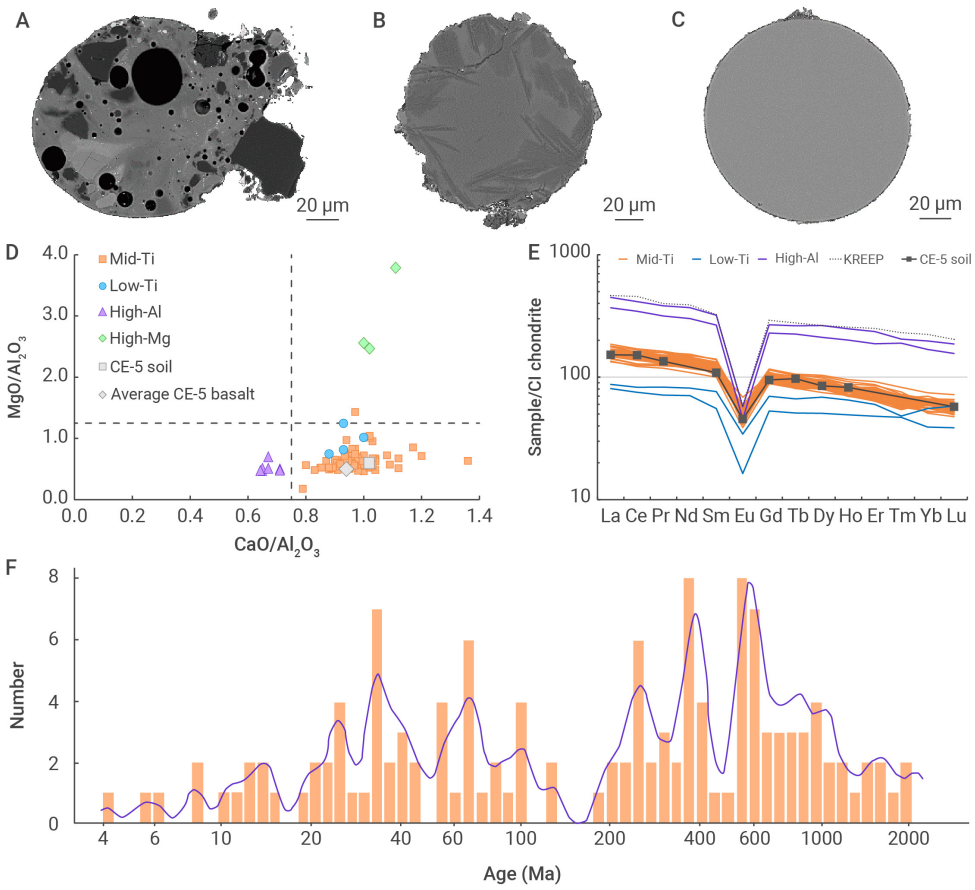

Figure 7. Textures, chemical compositions and ages of the CE-5 impact glasses (A-C) BSE images showing three typical textures: clast-bearing microbreccia; quenched crystallized glass and clean glass (after Yang W. et al. 2022[36]). (D) CaO/Al_2O_3 vs. MgO/Al_2O_3 diagram of the CE-5 glasses. The vertical dashed line highlights the CaO/Al_2O_3 ratio of 0.75 as a dividing line between basaltic (right) and high-Al glasses (left). The horizontal dashed line highlights a MgO/Al_2O_3 ratio of 1.25 as a dividing line between picritic (up) and basaltic glasses (down). Data are from Long et al. (2022),[34] Yang W. et al. (2022)[36] and Yan et al. (2022).[35] (E) REE concentrations of the CE-5 impact glasses normalized to CI chondrites.[104] KREEP data are from Warren and Taylor (2014).[105] The CE-5 soil data are from Li et al. (2022).[8] The impact glasses data are from Yang W. et al. (2022)[36] and Yan et al. (2022).[35] (F) Age distribution of CE-5 impact glasses with local compositions (after Long et al. 2022).[34]

olivine, and pyroclastic glass beads.[69,71] These clasts represent various rocks delivered by impact events from other un-sampled regions of the Moon, over ~50–400 km away from the CE-5 landing site.[71] In addition, a few impact-induced high-pressure minerals (i.e., seifertite and stishovite) were also identified in the CE-5 soil.[109] These high-pressure phases could represent the impact ejecta from relatively large impact craters, with 3–32 km diameters.[109] The lack of high-pressure phases in the CE-5 soil may suggest that impact conditions are unfavorable for preserving high-pressure phases on the Moon.[110] Moreover, a few impact-generated glass beads, compositionally distinct from the CE-5 basalt, have also been recognized in the CE-5 soil as exotic glass fragments (Figure 7D-E).[34–36] The formation, transport, and impact melting processes of these exotic impact glasses have been constrained using the geochemistry, microstructure, and U-Pb age data.[34–36]

Some of the exotic igneous clasts exhibit unusual characteristics compared with Apollo and Luna samples.[71] These clasts include: (1) a high-Ti vitrophyric fragment that shows a unique mineralogy among lunar basalts, probably representing a new type of lunar basalt; (2) a magnesian anorthosite clast represents a rock chip previously unrecognized in Apollo and Luna collections; (3) the pyroclastic glass records a compositional unique volcanic eruption on the Moon, i.e., low Mg# value and high FeO content (Figure 8).

Numerical modeling calculations and remote-sensing observations show that approximately 90% of the materials in the CE-5 regolith are expected to be sourced from the Em4/P58 unit, consistent with the observation of the CE-5 samples (~95%). A few exotic materials would be delivered from outside the Em4/P58 unit.[111–115] The potential major contributors of these exotic materials are Sharp B, Copernicus, Aristarchus, and Harding craters.[113–115] Ballistic sedimentation modeling results suggest that these four craters contributed less than 10% of the exotic materials in the CE-5 regolith.[113–115] Jia et al. (2022) suggested that these four craters could deliver a 0.05 m thick layer of primary ejecta to the CE-5 landing site, and then this ejecta further excavated about 0.46 m thick local materials.[113]

For the provenance of regolith sourced from inside of CE-5 basalt unit (Em4/P58 unit), remote-sensing observations and crater ejecta deposition models reveal that over 1800 impact craters in Em4/P58 unit likely deposited ~0.56 m of primary ejecta at the CE-5 landing site.[113] About 88% of this primary ejecta was contributed by 12 craters within 1 km from the CE-5 landing site.[113] Xu Guangqi crater, one of these 12 craters near the landing site, is the most volumetrically significant contributor (~0.3 m) to the CE-5 regolith.[113,114] In addition, the underlying low-Ti materials are also expected to be delivered to the CE-5 landing site.[113,114]

Although some exotic components have been identified in the CE-5 soil it is reasonable to predict that other specific exotic materials (e.g., new rock type, unique impact ejecta, and asteroid debris) may still exist in CE-5 collected sample. In the future, detailed investigations of these exotic components will improve our understanding of the surface process and magmatic evolution of the lunar crust.

SPACE WEATHERING

The CE-5 lunar samples owing to their high iron content and the middle latitude of sampling, also present an opportunity to study the features of lunar soil altered by space weathering.[21,26]

Microscopic morphology and crystallography of the altered lunar soil grains

Distinct microscopic morphological features are observed in the lunar soil grains. High-resolution electron microscopy was used to analyze the CE-5 impact glasses and mineral aggregates, revealing typical space weathering features, such as microcraters, impact-induced splashed melts, nano-sized adhesive mineral debris, and scattered metal beads.[35,37,120,121] Similar microstructures were previously observed in lunar soil samples from the Apollo and Luna missions.[122–126] In addition, the recent study by Yan et al. (2022)[35] recognized and classified abundant protruded and dented microstructures on a few glass particles, and the morphology and crosscutting relationship of the microstructures suggest that they were likely formed during regolith reworking by low-speed events (<2.4 km/s) of local materials with various thermophysical states (vapor, melt and solid). These observa-

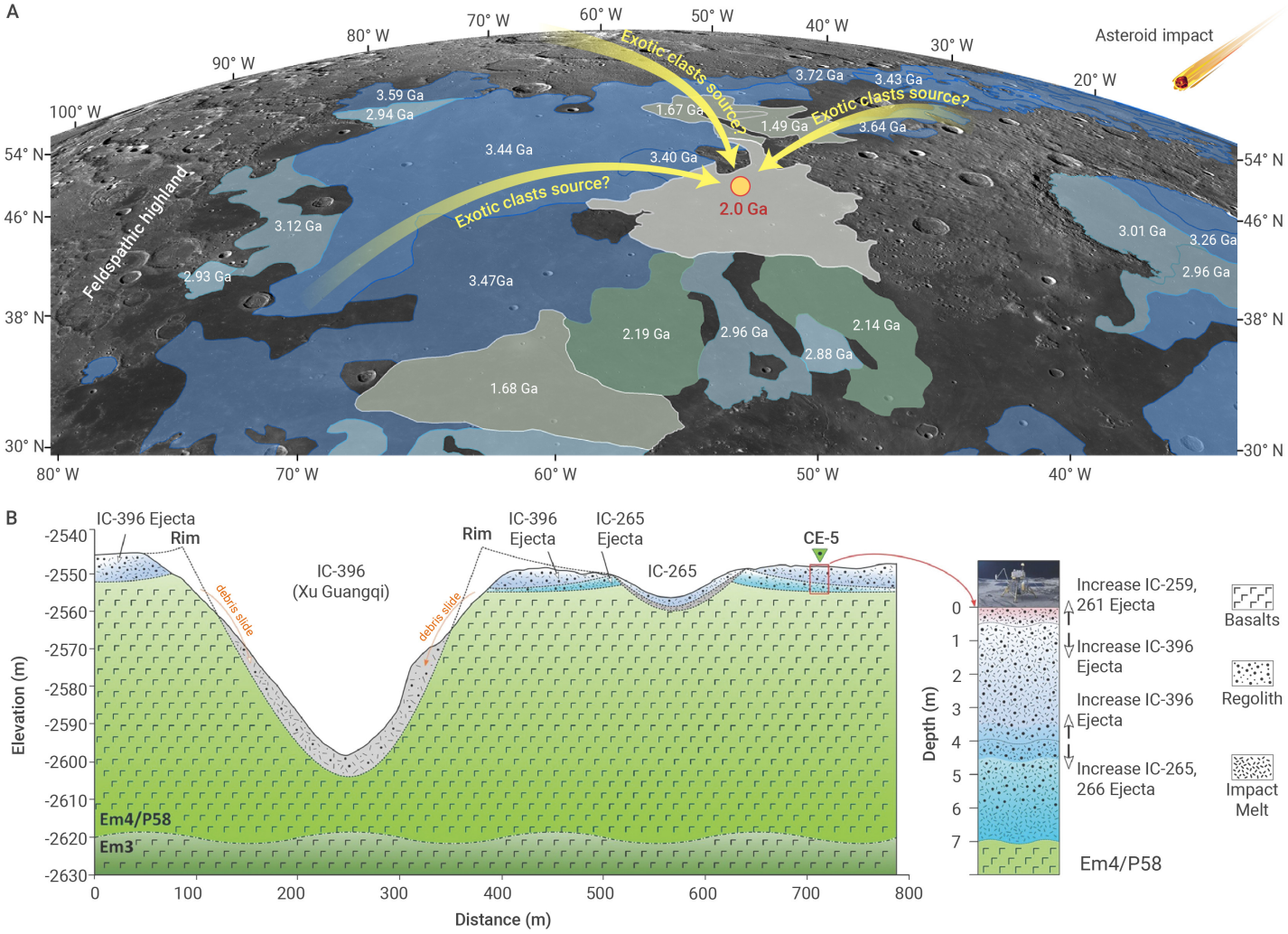

Figure 8. The provenance of the CE-5 soil (A) Image showing the provenance and exotic components for the CE-5 regolith. The colored areas represent the mare basalt units (defined by Hiesinger et al. 2011[10]). The 2.0 Ga age for the CE-5 basalt unit is reported by Che et al. (2021)[21] and Li Q. et al. (2021).[26] Exotic clasts are from other surrounding mare regions and highlands.[71] (B) Stratigraphy of Copernican-aged impact ejecta at the CE-5 landing site (after Qian et al. 2021[114]).

tions indicate that regolith reworking occurred mainly within the vicinity of the site. The findings are consistent with the results of theoretical models, which indicate that a small proportion (less than 10%) of the primary ejecta originated from a distance greater than 1 km from the CE-5 landing site.[113].

The lunar soil grains also suffer damage from the solar wind, which consists of the charged protons, helium, and other particles, that implant into their surfaces. FIB-TEM analysis of various phases (olivine, low-Ca and high-Ca pyroxene, plagioclase, phosphate, ilmenite, and sulfide) exposed on the surface of the same CE-5 basaltic clast demonstrated that the textures of the solar wind irradiation-damaged zone are dependent on the host mineral species, e.g., the size and abundance of nanophase iron particles ($npFe^0$) and the presence and shapes of helium bubbles.[37] The ilmenite grains from CE-5 soils have large quantities of helium bubbles in their glassy surface layer.[127] This discovery implies that the implanted helium can be extracted by mechanical crushing, providing insight into possible future *in situ* extraction of helium from the lunar soil.[127] While the solar wind radiation on the Moon is known to vary with latitude, the study of CE-5 lunar soils compared to Apollo samples found no significant latitude-dependent effects.[37]

Implantation and retention of the solar wind-derived water

Solar wind-derived water is one of the major water reservoirs on the Moon (e.g., ref.[128]). Global remote sensing revealed that water abundance (in the form of OH) increases with latitude, approaching ~500-700 ppm in the polar regions.[129] In addition, the surface water abundance of the Moon shows time-of-day variations.[129,130] To unravel the spatiotemporal distribution and retention of the solar wind-derived water in the lunar regolith, two parallel studies[42,43] have measured the D/H ratios and hydrogen content depth profiles in olivine, pyroxene, plagioclase and glass grains from CE-5 lunar soils. Hydrogen is predominantly concentrated in the outmost ~100 nm of the grains (with a maximum hydrogen content up to 1116 to 2516 ppm) and extremely depleted in deuterium (δD: −908 to 992 ‰), suggesting the implantation of solar wind. The hydrogen-content depth profiles are phase-dependent, bell-shaped for glass, or showing a monotonic decrease for crystals, which can be modeled by assuming dynamic equilibrium between implantation, diffusion, and outgassing of the solar wind hydrogen in the soil grains at the CE-5 landing site.[42] Combining the observations of Apollo and CE-5 soils, heating experiments, and theoretical simulations and modeling, the surface temperature on the Moon is likely to be a key factor controlling solar wind-hydrogen implantation and migration in lunar soils.[42,43] The solar wind-derived water (in the forms of H, OH and/or H_2O), preserved in the outmost ~100 nm grain rims, contributes a minimum of 170 ppm water abundance in the bulk CE-5 soils (Figure 9E). This value is comparable with the estimate measured by the *in situ* spectrometer on the lunar surface[64,131] and could be treated as "ground truth" for calibrating orbital spectral measurements.[129] Based on the dynamic equilibrium model established with the CE-5 and Apollo soil samples, a high abundance of solar wind-derived water in the finest lunar soils (<2 μm) of up to ~2 wt%, can be extrapolated at high latitude.[42] This discovery suggests a potential water resource on the Moon.

A recent study reported core-to-rim variations of water abundance and

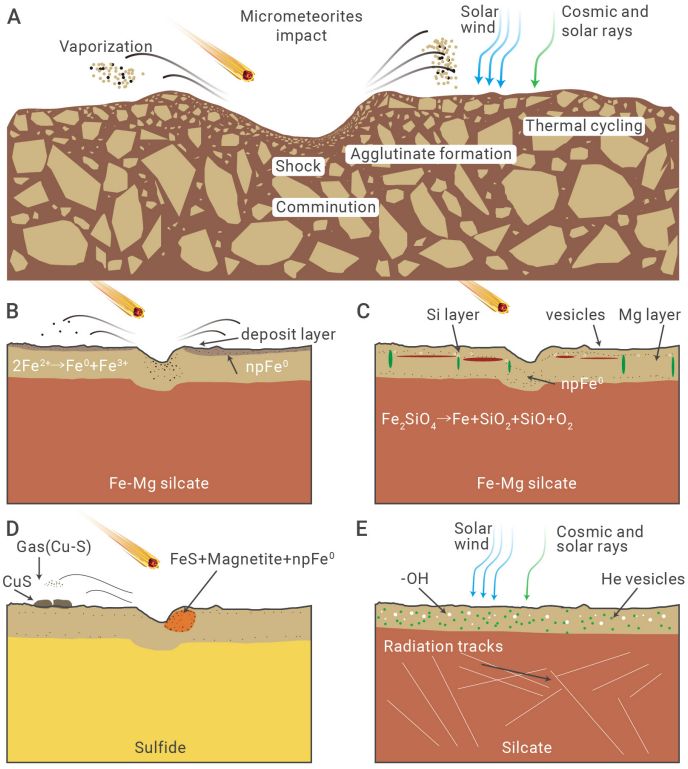

Figure 9. Conceptual diagrams depicting the space weathering processes, effects, and products observed at the CE-5 landing site (defined by refs.[37–43,116–119]) (A) Various mechanisms that contribute to space weathering, including micrometeorite impacts, energetic particle bombardment, and thermal fatigue. (B-C) The vaporization, in-situ reduction, and disproportion reactions producing np-Fe^0, SiO, and ferric ions in and around the micro-crater during micrometeorite impacts. (D) The alteration of sulfides during micrometeorite impacts, including the formation of np-Fe^0 and submicron magnetite via eutectic reaction, as well as the vapor-deposited digenite. (E) The implantation of energetic particles producing various products such as solar wind-origin water, helium vesicles, and radiation tracks.

D/H ratio in CE-5 impact glass beads,[132] in order to unravel the hydrated layer at depth in lunar soils.[133] The CE-5 impact glass beads contain 0~1,909 μg g^{-1} equivalent H_2O, and correlate negatively with H isotope compositions, ranging from −990 ± 6‰ to 522 ± 440‰. The observed correlation was interpreted by mixing solar wind-derived water with the intrinsic water hosted in the glass beads, implying that the impact glass beads can store solar wind derived water. Contrary to the degassing profiles of water recorded in the Apollo pyroclastic glasses,[134] the CE-5 impact glass beads show hydration profiles with water diffusing inwards. On the basis of these observations, He et al. (2023)[132] estimated that up to 2.7 × 10^{14} kg of solar wind-derived water is preserved in impact glass in lunar regolith, which plays a role as a buffer in the lunar surface water cycle.

Fe^0, Fe^{3+}, and the redox states of lunar soil

The Moon is known for its reduced environment, due to its low oxygen fugacity and lack of water, and for decades it was believed that npFe^0 was formed due to impact-induced vapor reduction.[118] Ferric irons were rarely found in lunar soil and were not previously considered indicators of space weathering products. Formation mechanisms of Fe^0 have been discovered in CE-5 lunar soil (Figure 9B-D). Recent studies have identified npFe^0 reduced by solar wind protons and those coexisting with wüstite nanoparticles by fayalitic olivine decomposition in CE-5 soil (Figure 9C).[37–39] In addition, both npFe^0 and ferric iron were found in microcraters on fayalite and in impact glass beads, believed to have been formed through the disproportionation reaction of ferrous irons (Figure 9B).[40,119] Furthermore, npFe^0 and magnetite have also been identified in micro-sized sulfide grains and are likely to have formed by eutectoid reactions (Figure 9D).[117] Notably, the disproportionation reaction is an entirely different formation mechanism of npFe^0, resulting from ferrous iron's self-redox reaction. The discovery of sub-micron magnetite in the sulfides of CE-5 lunar soil provides direct evidence for the presence of native magnetite in lunar soil. The presence of various types of ferric iron in CE-5 lunar soil has prompted a re-evaluation of the lunar redox environment during impacts, and potentially on other airless planetary bodies.

DEVELOPMENTS OF MICROANALYSIS TECHNIQUES

In the same manner as the Apollo Lunar Exploration Program promoted the development and application of scanning electron microscope (SEM) and secondary ion mass spectrometry (SIMS) 50 years ago,[135] the new lunar samples returned by the CE-5 mission once again set off a new wave of applications of microanalysis techniques in planetary science.[44] This renewed interest is not only due to the precious nature and micrometer size of the CE-5 samples, but also because microscopic and microspectroscopic techniques have undergone rapid advancements in the last two decades, promoting the development of Nanogeoscience and Planetary science.[136,137] Compared to relatively limited microanalysis abilities 50 years ago, the present-day microanalytical techniques have provided multi-scale morphological, structural, chemical, isotopic, and magnetic analyses on the tiny particles of CE-5 lunar soil samples. For instance, benefiting from the development of quantitative analysis methods based on Micro X-ray fluorescence (μXRF),[138] SEM coupled with energy-dispersive X-ray spectroscopy (SEM-EDXS),[139] and electron probe micro-analyzer (EPMA),[140] the chemical composition of micro-sized basalt fragments[29,31] and glass beads[36] from the CE-5 samples were quantitatively determined. First, the chemical composition of basalt fragments obtained from the EPMA and SEM-EDXS quantitative approaches was consistent with XRF measurement on powder samples of the CE-5 soil.[8] Second, owing to the improved analytic precise of SIMS and NanoSIMS,[141–143] the Pb/Pb geochronology on Zr-bearing minerals (less than 8 μm) from CE-5 basalt fragments yielded a precise age of the CE-5 basalts;[21,26] the hydrogen isotope compositions of apatite and ilmenite-hosted melt inclusions from the CE-5 basalts indicated that volcanism was not driven by abundant water in its mantle source.[23,42] Third, the coupled application of focused ion beam-scanning electron microscopy (FIB-SEM) and transmission electron microscopy (TEM) has provided new clues to the features and mechanisms of space weathering on the Moon. Gu and coworkers have found a phase-dependent effect on space weathering.[37] Two groups independently demonstrated the existence of Fe^{3+} in CE-5 samples.[40,119] These new findings suggest that most of the nanophase Fe on the Moon's surface might originate from impact-driven disproportionation.[37,40,119] Finally, three-dimension X-ray microscopy (3D XRM) has been used to non-destructively obtain the 3D morphology and internal structures of individual CE-5 particles at submicron resolution.[25,144]

The first wave of studies proves that advanced microanalysis techniques can accelerate research on the CE-5 lunar soil samples.[46] However, it is notable that unlocking as much information as possible from each targeted sample is critical and essential because these extraterrestrial samples are precious, small in size, and limited in quantity. Therefore, Li and coworkers developed a six-step workflow for correlatively and comprehensively studying CE-5 lunar samples and other extraterrestrial samples from a single particle on a nanometer to atomic scales.[45] By linking various microscopic and spectromicroscopic instruments together, this workflow consists of six steps: (1) selecting a single particle via a non-destructive μXRF technique, (2) characterizing 2D/3D morphology and structure with correlative submicron 3D XRM and nanoscale resolution FIB-SEM imaging methods, (3) analyzing the surface morphology and chemistry of the selected particle using SEM techniques, (4) obtaining structural, mineralogical, chemical, and isotopic features from the micron to nanometer scale via a series of microscopic and microbeam analyses on the cross-section of the selected particle, (5) determining a microregion of interest in the selected particle via advanced 2D/3D characterization and preparing thin foil/tip specimens using site-specific FIB cut, and (6) comprehensive analyses on the foil/tip specimens at nanometer to atomic scale with synchrotron-based scanning transmission X-ray microscopy (STXM), analytic TEM, and atom probe tomography (APT). Following this technical roadmap, one can integrate multiple modalities into a uniform frame of multimodal and multiscale correlated datasets to acquire high-throughput information on the limited or precious terrestrial and extraterrestrial samples. For example, step-(1)→ step-(4) has been used for identifying Zr-bearing minerals from individual basalt fragments and for

precise *in situ* SIMS Pb/Pb dating of various mineral phases.[26] Following a procedure of step-(1)→step-(3)→step-(5)→step-(6) studies on the morphology, structure, and chemistry of the selected particles at micron to atomic scales were determined to understand the process and mechanisms of space weathering.[37] By linking existing laboratory-based instruments, this workflow allows the establishment of rich multimodal and multiscale correlated datasets for mapping the local structure, mineralogy, chemistry, crystallography, and isotope geochemistry, as well as the local mechanical and magnetic performance across length scales.

It should be noted that some microanalysis techniques, such as synchrotron-based STXM and APT, have not been used to analyze the CE-5 samples although they were widely used in studies of meteorites and Apollo lunar samples.[145] Synchrotron-based STXM has the advantage of high spatial-resolution, high chemical-sensitivity, high quantity, and non-destructive X-ray microscopy and spectroscopy. Combined with X-ray absorption near-edge structure (XANES) and X-ray magnetic circular dichroism (XMCD), STXM can also be used to determine the oxidation state and magnetization of Fe in lunar soil samples.[146] APT can provide the 3D compositional mapping of materials with sub-nanometre spatial resolution, and its mass resolution is generally sufficient to distinguish each isotope of each detected element.[147] It has been used to characterize space-weathered ilmenite grain from Apollo 17 samples.[145] In the future, STXM and APT are expected to be the ideal analytical tools in lunar soil analysis projects. Generally, step-(6) could include three advanced microscopic approaches: STXM, TEM and APT. They are usually combined to obtain morphological, mineralogical, crystallographic, chemical (including isotopic and oxidization state), and magnetization information on the target foil or tip specimen at nanometer to atomic scale.[137] Furthermore, all the techniques mentioned in the six-step workflow can be combined to characterize precious samples from the Earth or other extraterrestrial bodies for a specific purpose.

SUMMARY AND PERSPECTIVE

This overview summarizes the main discoveries from the CE-5 lunar soil samples and, based on these, significant new understandings of the Moon. The studies also raise many new questions, specifically: What is the actual cause of the unusually long duration of volcanic activity in the CE-5 landing region? In addition, the CE-5 samples provide distinctive information in comparison to the Apollo and Luna samples. The CE-5 landing area is the youngest (2.03 Ga) and has a higher latitude (43°N). All reported basalt fragments in the CE-5 soil are local and likely crystallized from the same lava flow at different depths and cooling rates. Hence, the petrographic and geochemical study of this unique set of samples will establish a comprehensive model for the formation and evolution of mare basalts, including partial melting of the lunar mantle source, crystallization and differentiation during magma ascent, degassing and dehydration during the eruption on the lunar surface, and final cooling and solidification. The existing petrological, mineralogical and geochemical observations suggest that the CE-5 basalt was produced via a low degree of partial melting of the mantle source region, followed by a high degree of fractional crystallization, which could have produced significant isotopic fractionation, including various metal elements and volatile elements.

In addition, the CE-5 soils also contain a few percent of exotic materials, and this overview summarizes the findings of several Mg-suite lithic fragments. More exotic materials are expected to be found in the future study of the CE-5 lunar soil samples, which will reveal the geological features and evolutionary histories of a broad region beyond the Em4/P58 unit. Meanwhile, statistics of these exotic materials, combined with the regional geology and simulations of impact cratering events, will establish and test an impact model of material transportation and mixing on the lunar surface.

The CE-5 soils are dominated by the same basalt unit, Em4/P58, supplying suitable samples for the study of the surface processes on the Moon. It is worth noting that the CE-5 landing site is located at a middle latitude. Compared with the soils collected by Apollo and Luna missions at low latitudes, the latitude effect of space weathering on the Moon can be revealed for the first time, and a dynamic model of implantation, diffusion loss and migration of the solar wind in lunar regolith can be established. The formation and evolution model of lunar regolith can be constrained by systematic analyses of the lunar surface samples and the drill core, including isotope dating of a large number of impact glasses separated from the soils, determining the cosmic-ray exposure history of individual fragments and the bulk soils from different depths based on the cosmogenic noble gases and radioactive isotopes, and statistical analysis of solar energetic particle tracks in mineral grains. In addition, the high Ni contents of the bulk CE-5 soil indicate the presence of meteoritic materials. Separating and classifying the asteroid remnants preserved in the soils could yield the distribution pattern of the type of asteroids impacting the Moon in the past 2 billion years, providing a key constraint for planetary dynamic solar system evolution in combination with the asteroid impact flux.

The CE-6 mission is the backup of CE-5, and will land within the South Pole-Aitken basin (SPA, the largest and deepest impact basin on the Moon) and return samples in 2024. It may collect the first direct sample from the Moon's deep interior, and could provide strict constraints on lunar interior structure and composition and hence the Lunar Magma Ocean hypothesis. The impact flux before 4 Ga can be calibrated with returned impact melt samples of SPA, which will provide critical evidence for or against the Late Heavy Bombardment hypothesis. Also noteworthy is that study of the first samples from the lunar farside, compared with the CE-5 soils and previous Apollo and Luna samples from the nearside, will also test the hypothesis that the Moon has been irradiated by the Earth's wind.

REFERENCES

1. Kring, D.A., Durda, D.D. (2012). A global lunar landing site study to provide the scientific context for exploration of the Moon (Lunar and Planetary Institute).
2. National Research Council (2007). The scientific context for exploration of the Moon (The National Academies Press).
3. Giguere, T.A., Taylor, G.J., Hawke, B.R., et al. (2000). The titanium contents of lunar mare basalts. Meteorit. Planet. Sci. ***35***, 193–200.
4. Tartèse, R., Anand, M., Gattacceca, J., et al. (2019). Constraining the evolutionary history of the Moon and the inner solar system: A case for new returned lunar samples. Space Sci. Rev. ***215***, 54.
5. Xiao, L., Head, J.W. (2020). Geological characteristics of the Moon.
6. Hu, H., Pei, Z., Li, C., et al. (2021). Overall design of unmanned lunar sampling and return project—Chang'e-5 mission. Sci. Sin. Technol. ***51***, 1275–1286.
7. Yang, M., Zhang, G., Zhang, W., et al. (2021). Technical design and implementation of Chang'e-5 robotic sample return mission on lunar surface. Sci. Sin. Technol. ***51***, 738–752.
8. Li, C., Hu, H., Yang, M.-F., et al. (2022). Characteristics of the lunar samples returned by the Chang'E-5 mission. Natl. Sci. Rev. ***9***, nwab188.
9. Qian, Y.Q., Xiao, L., Zhao, S.Y., et al. (2018). Geology and scientific significance of the Rümker region in northern Oceanus Procellarum: China's Chang'E-5 landing region. J. Geophys. Res. Planets ***123***, 1407–1430.
10. Hiesinger, H., Head, J.W., Wolf, U., et al. (2011). Ages and stratigraphy of lunar mare basalts: A synthesis. Spec. Pap. Geol. Soc. Am. ***477***, 1–51.
11. Du, J., Fa, W., Gong, S., et al. (2022). Thicknesses of mare basalts in the Chang'E-5 landing region: Implications for the late-stage volcanism on the Moon. J. Geophys. Res. Planets ***127***, e2022JE007314.
12. Qian, Y., Xiao, L., Head, J.W., et al. (2021). Young lunar mare basalts in the Chang'e-5 sample return region, northern Oceanus Procellarum. Earth Planet. Sci. Lett. ***555***, 116702.
13. Giguere, T.A., Boyce, J.M., Gillis-Davis, J.J., et al. (2022). Lava flow ages in northeastern Oceanus Procellarum: The need for calibrating crater counting procedures. Icarus ***375***, 114838.
14. Jia, M., Yue, Z., Di, K., et al. (2020). A catalogue of impact craters larger than 200 m and surface age analysis in the Chang'e-5 landing area. Earth Planet. Sci. Lett. ***541***, 116272.
15. Morota, T., Haruyama, J., Ohtake, M., et al. (2011). Timing and characteristics of the latest mare eruption on the Moon. Earth Planet. Sci. Lett. ***302***, 255–266.
16. Cao, K., Dong, M., She, Z., et al. (2022). A novel method for simultaneous analysis of particle size and mineralogy for Chang'E-5 lunar soil with minimum sample consumption. Sci. China Earth Sci. ***65***, 1704–1714.
17. Fu, X., Yin, C., Jolliff, B.L., et al. (2022). Understanding the mineralogy and geochemistry of Chang'E-5 soil and implications for its geological significances. Icarus, 115254.
18. Yao, Y., Xiao, C., Wang, P., et al. (2022). Instrumental neutron activation analysis of Chang'E-5 lunar regolith samples. J. Am. Chem. Soc. ***144***, 5478–5484.
19. Zhang, H., Zhang, X., Zhang, G., et al. (2021). Size, morphology, and composition of lunar samples returned by Chang'E-5 mission. Sci. China Phys. Mech. Astron. ***65***, 229511.
20. Zong, K., Wang, Z., Li, J., et al. (2022). Bulk compositions of the Chang'E-5 lunar soil: Insights into chemical homogeneity, exotic addition, and origin of landing site basalts. Geochim. Cosmochim. Acta ***335***, 284–296.
21. Che, X., Nemchin, A., Liu, D., et al. (2021). Age and composition of young basalts on the Moon, measured from samples returned by Chang'e-5. Science ***374***, 887–890.

22. He, Q., Li, Y., Baziotis, I., et al. (2022). Detailed petrogenesis of the unsampled Oceanus Procellarum: The case of the Chang'e-5 mare basalts. Icarus ***383***, 115082.
23. Hu, S., He, H., Ji, R., et al. (2021). A dry lunar mantle reservoir for young mare basalts of Chang'e-5. Nature ***600***, 49–53.
24. Ji, J., He, H., Hu, S., et al. (2022). Magmatic chlorine isotope fractionation recorded in apatite from Chang'e-5 basalts. Earth Planet. Sci. Lett. ***591***, 117636.
25. Jiang, Y., Li, Y., Liao, S., et al. (2022). Mineral chemistry and 3D tomography of a Chang'E 5 high-Ti basalt: implication for the lunar thermal evolution history. Sci. Bull. ***67***, 755–761.
26. Li, Q.-L., Zhou, Q., Liu, Y., et al. (2021). Two-billion-year-old volcanism on the Moon from Chang'e-5 basalts. Nature ***600***, 54–58.
27. Liu, D., Wang, X., Liu, J., et al. (2022). Spectral interpretation of late-stage mare basalt mineralogy unveiled by Chang'E-5 samples. Nat. Commun. ***13***, 5965.
28. Qian, Y., She, Z., He, Q., et al. (2023). Mineralogy and chronology of the young mare volcanism in the Procellarum-KREEP-Terrane. Nat. Astron. ***7***, 287–297.
29. Su, B., Yuan, J., Chen, Y., et al. (2022). Fusible mantle cumulates trigger young mare volcanism on the cooling Moon. Sci. Adv. ***8***, eabn2103.
30. Tian, H., Yang, W., Zhang, D., et al. (2022). Petrogenesis of Chang'E-5 mare basalts: Clues from the trace elements. Am. Mineral. (in press).
31. Tian, H.-C., Wang, H., Chen, Y., et al. (2021). Non-KREEP origin for Chang'e-5 basalts in the Procellarum KREEP Terrane. Nature ***600***, 59–63.
32. Wang, Z., Wang, W.-(RZ), Tian, W., et al. (2023). Cooling rate of clinopyroxene reveals the thickness and effusion volume of Chang'E-5 basaltic flow units. Icarus ***394***, 115406.
33. Zhang, D., Su, B., Chen, Y., et al. (2022). Titanium in olivine reveals low-Ti origin of the Chang'E-5 lunar basalts. Lithos ***414–415***, 106639.
34. Long, T., Qian, Y., Norman, M.D., et al. (2022). Constraining the formation and transport of lunar impact glasses using the ages and chemical compositions of Chang'e-5 glass beads. Sci. Adv. ***8***, eabq2542.
35. Yan, P., Xiao, Z., Wu, Y., et al. (2022). Intricate regolith reworking processes revealed by microstructures on lunar impact glasses. J. Geophys. Res. Planets ***127***, e2022JE007260.
36. Yang, W., Chen, Y., Wang, H., et al. (2022). Geochemistry of impact glasses in the Chang'e-5 regolith: Constraints on impact melting and the petrogenesis of local basalt. Geochim. Cosmochim. Acta ***335***, 183–196.
37. Gu, L., Chen, Y., Xu, Y., et al. (2022). Space weathering of the Chang'e-5 lunar sample from a mid-high latitude region on the Moon. Geophys. Res. Lett. ***49***, e2022GL097875.
38. Guo, J.-G., Ying, T., Gao, H., et al. (2022). Surface microstructures of lunar soil returned by Chang'e-5 mission reveal an intermediate stage in space weathering process. Sci. Bull. ***67***, 1696–1701.
39. Guo, Z., Li, C., Li, Y., et al. (2022). Nanophase iron particles derived from fayalitic olivine decomposition in Chang'E-5 lunar soil: Implications for thermal effects during impacts. Geophys. Res. Lett. ***49***, e2021GL097323.
40. Li, C., Guo, Z., Li, Y., et al. (2022). Impact-driven disproportionation origin of nanophase iron particles in Chang'e-5 lunar soil sample. Nat. Astron. ***6***, 1156–1162.
41. Mo, B., Guo, Z., Li, Y., et al. (2022). In situ investigation of the valence states of iron-bearing phases in Chang'E-5 lunar soil using FIB, AES, and TEM-EELS Techniques. At. Spectrosc. ***43***, 53–59.
42. Xu, Y., Tian, H.-C., Zhang, C., et al. (2022). High abundance of solar wind-derived water in lunar soils from the middle latitude. Proc. Natl. Acad. Sci. ***119***, e2214395119.
43. Zhou, C., Tang, H., Li, X., et al. (2022). Chang'E-5 samples reveal high water content in lunar minerals. Nat. Commun. ***13***, 5336.
44. Li, J.H., Yang, W., Li, X.Y., et al. (2022). The Chang'e-5 lunar samples stimulate the development of microanalysis techniques. At. Spectrosc. ***43***, 1–5.
45. Li, J.-H., Li, Q.-L., Zhao, L., et al. (2022). Rapid screening of Zr-containing particles from Chang'e-5 lunar soil samples for isotope geochronology: Technical roadmap for future study. Geosci. Front. ***13***, 101367.
46. Yang, W., Li, J.H., Li, X.Y., et al. (2022). Microanalysis techniques guarantee long-term research On Chang'e-5 lunar samples. At. Spectrosc. ***43***, 266–271.
47. Lucey, P.G., Blewett, D.T., Jolliff, B.L. (2000). Lunar iron and titanium abundance algorithms based on final processing of Clementine ultraviolet-visible images. J. Geophys. Res. Planets ***105***, 20297–20305.
48. Carrier, W.D., Olhoeft, G.R., Mendell, W. (1991). Physical properties of the lunar surface. In Lunar Sourcebook: A user's guide to the Moon (Cambridge University Press), pp. 475–594.
49. McKay, D.S., Fruland, R.M., Heiken, G.H. (1974). Grain size and the evolution of lunar soils. In 5th Lunar Science Conference, pp. 887–906.
50. Cadenhead, D.A., Stetter, J.R. (1975). Specific gravities of lunar materials using helium pycnometry. In 6th Lunar Science Conference, pp. 3199–3206.
51. Gammage, R.B., Holmes, H.F. (1975). Specific surface area as a maturity index of lunar fines. Earth Planet. Sci. Lett. ***27***, 424–426.
52. Holmes, H.F., Fuller, E.L.Jr., Gammage, R.B. (1973). Interaction of gases with lunar materials: Apollo 12, 14, and 16 Samples. In 4th Lunar Science Conference, pp. 2413-2423.
53. Robens, E., Bischoff, A., Schreiber, A., Unger, K.K. (2008). Investigation of surface properties of lunar regolith part III. J. Therm. Anal. Calorim. ***94***, 627–631.
54. Staid, M.I., Pieters, C.M., Besse, S., et al. (2011). The mineralogy of late stage lunar volcanism as observed by the Moon Mineralogy Mapper on Chandrayaan-1. J. Geophys. Res. Planets ***116***.
55. Xu, R., Li, C., Yuan, L., et al. (2022). Lunar mineralogical spectrometer on Chang'E-5 mission. Space Sci. Rev. ***218***, 41.
56. Xu, J., Wang, M., Lin, H., et al. (2022). In-Situ photometric properties of lunar regolith revealed by lunar mineralogical spectrometer on board Chang'E-5 lander. Geophys. Res. Lett. ***49***, e2021GL096876.
57. Yang, Y., Jiang, T., Liu, Y., et al. (2022). A micro mid-infrared spectroscopic study of Chang'e-5 sample. J. Geophys. Res. Planets ***127***, e2022JE007453.
58. Pieters, C.M., Taylor, L.A., Noble, S.K., et al. (2000). Space weathering on airless bodies: Resolving a mystery with lunar samples. Meteorit. Planet. Sci. ***35***, 1101–1107.
59. Pieters, C.M., Boardman, J., Buratti, B., et al. (2009). The Moon Mineralogy Mapper (M3) on Chandrayaan-1. Curr. Sci. ***96***, 500–505.
60. Pieters, C.M., Noble, S.K. (2016). Space weathering on airless bodies. J. Geophys. Res. Planets ***121***, 1865–1884.
61. Wu, X., Liu, Y., Yang, Y., et al. (2022). Mineralogy and regolith maturity at the Chang'E-5 landing site inferred from the Lunar Mineralogical Spectrometer. Earth Planet. Sci. Lett. ***594***, 117747.
62. Trang, D., Lucey, P.G. (2019). Improved space weathering maps of the lunar surface through radiative transfer modeling of Kaguya multiband imager data. Icarus ***321***, 307–323.
63. Lu, X., Chen, J., Ling, Z., et al. (2023). Mature lunar soils from Fe-rich and young mare basalts in the Chang'e-5 regolith samples. Nat. Astron. ***7***, 142–151.
64. Lin, H., Li, S., Xu, R., et al. (2022). In situ detection of water on the Moon by the Chang' E-5 lander. Sci. Adv. ***8***, eabl9174.
65. Li, S., Milliken, R.E. (2016). An empirical thermal correction model for Moon Mineralogy Mapper data constrained by laboratory spectra and Diviner temperatures. J. Geophys. Res. Planets ***121***, 2081–2107.
66. Lin, H., Li, S., Lin, Y., et al. (2021). Thermal modeling of the lunar regolith at the Chang' E-4 landing site. Geophys. Res. Lett. ***48***, e2020GL091687.
67. McKay, D.S., Heiken, G.H., Basu, A., et al. (1991). The lunar regolith. In Lunar Sourcebook: A user's guide to the Moon (Cambridge University Press), pp. 285–356.
68. Yang, W., Wang, Y., Gao, L., et al. (2022). Sci-tech arts on Chang'e-5 lunar soil. The Innovation ***3***, 100300.
69. Sheng, S., Chen, Y., Zhang, B., et al. (2022). First location and characterization of lunar highland clasts in Chang'E-5 breccias using TIMA-SEM-EPMA. At. Spectrosc. ***43***, 351–362.
70. Yang, J., Ju, D., Pang, R., et al. (2023). Significance of silicate liquid immiscibility for the origin of young highly evolved lithic clasts in Chang'E-5 regolith. Geochim. Cosmochim. Acta ***340***, 189–205.
71. Zeng, X., Li, X., Liu, J. (2022). Exotic clasts in Chang'e-5 regolith indicative of unexplored terrane on the Moon. Nat. Astron. ***7***, 152–159.
72. Jiang, Y., Kang, J., Liao, S., et al. (2023). Fe and Mg isotope compositions indicate a hybrid mantle source for young chang'e 5 mare basalts. Astrophys. J. Lett. ***945***, L26.
73. Yuan, J., Huang, H., Chen, Y., et al. (2023). Automatic bulk composition analysis of lunar basalts: novel big-data algorithm for energy-dispersive x-ray spectroscopy. ACS Earth Space Chem. ***7***, 370–378.
74. Neal, C.R., Taylor, L.A. (1992). Petrogenesis of mare basalts: A record of lunar volcanism. Geochim. Cosmochim. Acta ***56***, 2177–2211.
75. Shearer, C.K., Hess, P.C., Wieczorek, M.A., et al. (2006). Thermal and magmatic evolution of the Moon. Rev. Mineral. Geochem. ***60***, 365–518.
76. Warner, R.D., Nehru, C.E., Keil, K. (1978). Opaque oxide mineral crystallization in lunar high-titanium mare basalts. Am. Mineral. ***63***, 1209–1224.
77. Yue, Z., Di, K., Michael, G., et al. (2022). Martian surface dating model refinement based on Chang'E-5 updated lunar chronology function. Earth Planet. Sci. Lett. ***595***, 117765.
78. Yue, Z., Di, K., Wan, W., et al. (2022). Updated lunar cratering chronology model with the radiometric age of Chang'e-5 samples. Nat. Astron. ***6***, 541–545.
79. Neukum, G. (1983). Meteorite Bombardment and Dating of Planetary Surfaces.
80. Papike, J.J., Hodges, F.N., Bence, A.E., et al. (1976). Mare basalts: crystal chemistry, mineralogy, and petrology. Rev. Geophys. ***14***, 475–540.
81. Borg, L.E., Shearer, C.K., Asmerom, Y., Papike, J.J. (2004). Prolonged KREEP magmatism on the Moon indicated by the youngest dated lunar igneous rock. Nature ***432***, 209–211.
82. Snyder, G.A., Taylor, L.A., Neal, C.R. (1992). A chemical model for generating the sources of mare basalts: Combined equilibrium and fractional crystallization of the lunar magmasphere. Geochim. Cosmochim. Acta ***56***, 3809–3823.
83. Borg, L.E., Gaffney, A.M., Shearer, C.K., DePaolo, D.J., et al. (2009). Mechanisms for incompatible-element enrichment on the Moon deduced from the lunar basaltic meteorite Northwest Africa 032. Geochim. Cosmochim. Acta ***73***, 3963–3980.
84. Luo, B., Wang, Z., Song, J., et al. (2023). The magmatic architecture and evolution of the Chang'e-5 lunar basalts. Nat. Geosci. ***16***, 301–308.
85. Yang, W., Lin, Y. (2021). New lunar samples returned by Chang'e-5: Opportunities for new discoveries and international collaboration. The Innovation ***2***, 100070.
86. Filiberto, J., Treiman, A.H. (2009). Martian magmas contained abundant chlorine, but little water. Geology ***37***, 1087–1090.
87. Liu, X., Hao, J., Li, R.-Y., et al. (2022). Sulfur isotopic fractionation of the youngest Chang'e-5 Basalts: Constraints on the magma degassing and geochemical features of the mantle source. Geophys. Res. Lett. ***49***, e2022GL099922.
88. Gargano, A., Sharp, Z., Shearer, C., et al. (2020). The Cl isotope composition and halogen contents of Apollo-return samples. Proc. Natl. Acad. Sci. ***117***, 23418–23425.
89. Sharp, Z.D., Shearer, C.K., McKeegan, K.D., et al. (2010). The chlorine isotope composition of the Moon and implications for an anhydrous mantle. Science ***329***, 1050–1053.
90. Boyce, J.W., Tomlinson, S.M., McCubbin, F.M., et al. (2014). The Lunar Apatite Paradox. Science ***344***, 400–402.
91. McCubbin, F.M., Vander Kaaden, K.E., Tartèse, R., et al. (2015). Experimental investigation of F, Cl, and OH partitioning between apatite and Fe-rich basaltic melt at 1.0–1.2 GPa and 950–1000 °C†. Am. Mineral. ***100***, 1790–1802.

92. McCubbin, F.M., Kaaden, K.E.V., Tartèse, R., et al. (2015). Magmatic volatiles (H, C, N, F, S, Cl) in the lunar mantle, crust, and regolith: Abundances, distributions, processes, and reservoirs. Am. Mineral. ***100***, 1668–1707.
93. Delano, J.W. (1986). Pristine lunar glasses: Criteria, data, and implications. J. Geophys. Res. Solid Earth ***91***, 201–213.
94. Korotev, R.L., Zeigler, R.A., Floss, C. (2010). On the origin of impact glass in the Apollo 16 regolith. Geochim. Cosmochim. Acta ***74***, 7362–7388.
95. Norman, M.D., Jourdan, F., Hui, S.S.M. (2019). Impact history and regolith evolution on the Moon: Geochemistry and ages of glasses from the Apollo 16 site. J. Geophys. Res. Planets ***124***, 3167–3180.
96. Naney, M.T., Crowl, D.M., Papike, J.J. (1976). The Apollo 16 drill core: Statistical analysis of glass chemistry and the characterization of a high alumina-silica poor (HASP) glass. Lunar Planet. Sci. Conf. Proc. ***1***, 155–184.
97. Delano, J.W., Lindsley, D.H., Rudowski, R. (1982). Glasses of impact origin from Apollo 11, 12, 15, and 16: Evidence for fractional vaporization and mare/highland mixing. Lunar Planet. Sci. Conf. Proc. ***1***, 339–370.
98. Delano, J.W., Zellner, N.E.B., BarraA, F., et al. (2007). An integrated approach to understanding Apollo 16 impact glasses: Chemistry, isotopes, and shape. Meteorit. Planet. Sci. ***42***, 993–1004.
99. Huang, Y.-H., Minton, D.A., Zellner, N.E.B., et al. (2018). No change in the recent lunar impact flux required based on modeling of impact glass spherule age distributions. Geophys. Res. Lett. ***45***, 6805–6813.
100. Norman, M.D., Adena, K.J.D., Christy, A.G. (2012). Provenance and Pb isotopic ages of lunar volcanic and impact glasses from the Apollo 17 landing site. Aust. J. Earth Sci. ***59***, 291–306.
101. Zellner, N.E.B. (2019). Lunar impact glasses: probing the Moon's surface and constraining its impact history. J. Geophys. Res. Planets ***124***, 2686–2702.
102. Zellner, N.E.B., Delano, J.W. (2015). 40Ar/39Ar ages of lunar impact glasses: Relationships among Ar diffusivity, chemical composition, shape, and size. Geochim. Cosmochim. Acta ***161***, 203–218.
103. Zellner, N.E.B., Spudis, P.D., Delano, J.W., Whittet, D.C.B. (2002). Impact glasses from the Apollo 14 landing site and implications for regional geology. J. Geophys. Res. Planets ***107***, 12–1.
104. McDonough, W.F., Sun, S. -s. (1995). The composition of the Earth. Chem. Evol. Mantle ***120***, 223–253.
105. Warren, P.H., Taylor, G.J. (2014). 2.9 - The Moon. In Treatise on Geochemistry (Second Edition), H. D. Holland and K. K. Turekian, eds. (Elsevier), pp. 213–250.
106. Anders, E., Ganapathy, R., Krähenbühl, U., Morgan, J.W. (1973). Meteoritic material on the Moon. The Moon ***8***, 3–24.
107. Wasson, J.T., Boynton, W.V., Chou, C.-L., Baedecker, P.A. (1975). Compositional evidence regarding the influx of interplanetary materials onto the lunar surface. The Moon ***13***, 121–141.
108. Cao, H., Wang, C., Chen, J., et al. (2022). A Raman spectroscopic and microimage analysis perspective of the Chang'e-5 lunar samples. Geophys. Res. Lett. ***49***, e2022GL099282.
109. Pang, R., Yang, J., Du, W., et al. (2022). New occurrence of seifertite and stishovite in Chang'E-5 regolith. Geophys. Res. Lett. ***49***, e2022GL098722.
110. Xing, W., Lin, Y., Zhang, C., et al. (2020). Discovery of reidite in the lunar meteorite Sayh al Uhaymir 169. Geophys. Res. Lett. ***47***, e2020GL089583.
111. Fu, X., Hou, X., Zhang, J., et al. (2021). Possible non-mare lithologies in the regolith at the Chang'E-5 landing site: Evidence from remote sensing data. J. Geophys. Res. Planets ***126***, e2020JE006797.
112. Hou, X., Fu, X., Qiao, L., et al. (2022). Absolute model ages of three craters in the vicinity of the Chang'E-5 landing site and their geologic implications. Icarus ***372***, 114730.
113. Jia, B., Fa, W., Zhang, M., et al. (2022). On the provenance of the Chang'E-5 lunar samples. Earth Planet. Sci. Lett. ***596***, 117791.
114. Qian, Y., Xiao, L., Head, J.W., et al. (2021). Copernican-Aged (<200 Ma) impact ejecta at the Chang'e-5 landing site: Statistical evidence from crater morphology, morphometry, and degradation models. Geophys. Res. Lett. ***48***, e2021GL095341.
115. Xie, M., Xiao, Z., Zhang, Xu, A. (2020). The provenance of regolith at the Chang'e-5 candidate landing region. J. Geophys. Res. Planets ***125***, e2019JE006112.
116. Guo, Z., Li, C., Li, Y., et al. (2023). Vapor-deposited digenite in Chang'e-5 lunar soil. Sci. Bull. ***68***, 723–729.
117. Guo, Z., Li, C., Li, Y., et al. (2022). Sub-microscopic magnetite and metallic iron particles formed by eutectic reaction in Chang'E-5 lunar soil. Nat. Commun. ***13***, 7177.
118. Keller, L.P., McKay, D.S. (1993). Discovery of vapor deposits in the lunar regolith. Science ***261***, 1305–1307.
119. Xian, H., Zhu, J., Yang, Y., et al. (2023). Ubiquitous and progressively increasing ferric iron content on the lunar surfaces revealed by the Chang'e-5 sample. Nat. Astron. ***7***, 280–286.
120. Gu, Y., Sun, J., Xiao, Q., et al. (2022). Morphology of lunar soil returned by chang'e-5 mission and implications for space weathering. Earth Sci. ***47***, 4145–4160.
121. Li, C., Li, Y., Wei, K., et al. (2023). Study on surface characteristics of Chang'E-5 fine grained lunar soil. Sci. Sin. Phys. Mech. Astron. ***53***, 239603.
122. Carter, J.L., MacGregor, I.D. (1970). Mineralogy, petrology and surface features of some Apollo 11 samples. Geochim. Cosmochim. Acta Suppl. ***1***, 247.
123. Carter, J.L. (1971). Chemistry and surface morphology of fragments from Apollo 12 soil. Lunar Planet. Sci. Conf. Proc. ***2***, 873.
124. Carter, J.L. (1973). Chemistry and surface morphology of soil particles from Luna 20 LRL sample 22003. Geochim. Cosmochim. Acta ***37***, 795–803.
125. Carter, J.L., McKay, D.S. (1971). Influence of target temperature on crater morphology and implications on the origin of craters on lunar glass spheres. Lunar Planet. Sci. Conf. Proc. ***2***, 2653.
126. Carter, J.L., McKay, D.S. (1972). Metallic mounds produced by reduction of material of simulated lunar composition and implications on the origin of metallic mounds on lunar glasses. Lunar Planet. Sci. Conf. Proc. ***3***, 953.
127. Li, A., Chen, X., Song, L., et al. (2022). Taking advantage of glass: capturing and retaining the helium gas on the Moon. Mater. Futur. ***1***, 035101.
128. Jones, B.M., Aleksandrov, A., Hibbitts, K., et al. (2018). Solar wind-induced water cycle on the Moon. Geophys. Res. Lett. ***45***, 10,959–10,967.
129. Li, S., Milliken, R.E. (2017). Water on the surface of the Moon as seen by the Moon Mineralogy Mapper: Distribution, abundance, and origins. Sci. Adv. ***3***, e1701471.
130. Wöhler, C., Grumpe, A., Berezhnoy, A.A., et al. (2017). Temperature regime and water/hydroxyl behavior in the crater Boguslawsky on the Moon. Icarus ***285***, 118–136.
131. Liu, J., Liu, B., Ren, X., et al. (2022). Evidence of water on the lunar surface from Chang'E-5 in-situ spectra and returned samples. Nat. Commun. ***13***, 3119.
132. He, H., Ji, J., Zhang, Y., et al. (2023). A solar wind-derived water reservoir on the Moon hosted by impact glass beads. Nat. Geosci. ***16***, 294–300.
133. Benna, M., Hurley, D.M., Stubbs, T.J., et al. (2019). Lunar soil hydration constrained by exospheric water liberated by meteoroid impacts. Nat. Geosci. ***12***, 333–338.
134. Saal, A.E., Hauri, E.H., Cascio, M.L., et al. (2008). Volatile content of lunar volcanic glasses and the presence of water in the Moon's interior. Nature ***454***, 192–195.
135. Li, Q.L. (2015). Characteristics and analytical methods of the U-Pb dating system. Bull. Mineral. Petrol. Geochem. ***34***, 491–500.
136. Hochella, M.F., Lower, S.K., Maurice, P.A., et al. (2008). Nanominerals, mineral nanoparticles, and earth systems. Science ***319***, 1631–1635.
137. Li, J.H., Pan, Y.X. (2015). Applications of transmission electron microscopy in the earth sciences. Sci. Sin. Terrae ***45***, 1359–1382.
138. Liu, Y., Zhang, C., Zhang, D., et al. (2022). Non-destructive micro X-ray fluorescence quantitative analysis of geological materials. At. Spectrosc. ***43***, 378–387.
139. Yuan, J.Y., Chen, Y., Zhang, D., et al. (2022). Quantitative analysis of bulk composition of small-size lunar samples using energy dispersive x-ray spectroscopy. At. Spectrosc. ***43***, 292–302.
140. Zhang, D., Chen, Y., Yang, W., et al. (2022). High-precision measurement of trace level Na. In and Ni in lunar glass using electron probe microanalysis. At. Spectrosc. ***43***, 28–41.
141. Hao, J., Hu, S., Li, R.Y., et al. (2022). High precision and resolution chlorine isotopic analysis of apatite using NanoSIMS. At. Spectrosc. ***43***, 321–328.
142. Li, Y., Tang, G.Q., Hsu, W.B., Wu, Y.H. (2022). In situ SIMS carbon isotopic analysis of carbon-bearing minerals in nantan and aletai iron meteorites: Implications on genesis. At. Spectrosc. ***43***, 329–336.
143. Liu, Y., Li, X.H., Savage, P.S., et al. (2022). New quartz and zircon si isotopic reference materials for precise and accurate SIMS isotopic microanalysis. At. Spectrosc. ***43***, 99–106.
144. Zhang, C., Li, J.H. (2022). Non-destructive identification and quantification of ilmenite from a single particle of the Chang'e-5 lunar soil sample. At. Spectrosc. ***43***, 284–291.
145. Greer, J., Rout, Surya.S., et al. (2020). Atom probe tomography of space-weathered lunar ilmenite grain surfaces. Meteorit. Planet. Sci. ***55***, 426–440.
146. Wang, J., Li, J.H. (2022). Scanning transmission X-ray microscopy at the Canadian Light Source: Progress and selected applications in geoscience. At. Spectrosc. ***43***, 84–98.
147. Miller, M.K., Forbes, R.G. (2009). Atom probe tomography. Mater. Charact. ***60***, 461–469.

ACKNOWLEDGMENTS

We thank James W. Head for editing and language polishing and Randy L. Korotev for constructive comments and suggestions. This work is jointly supported by the National Natural Science Foundation of China (42241103, 42241104), the Strategic Priority Research Program of Chinese Academy of Sciences (XDB 41000000), the key research program of Chinese Academy of Sciences (ZDBS-SSW-JSC007), and the key research program of the Institute of Geology and Geophysics, Chinese Academy of Sciences (IGGCAS-202101), and Pre-research project on Civil Aerospace Technologies by CNSA (D020201 and D020203).

AUTHOR CONTRIBUTIONS

Y.L., C.L. and X.-H.L. supervised and revised the manuscript. Y.C., S.H., J.-H.L., X.L., Y.Li, Y.Liu, Y.Q., W.Y., and Q.Z. wrote and edited the manuscript. All authors contributed to the article and approved the submitted version.

DECLARATION OF INTERESTS

The authors declare no competing interests.

LEAD CONTACT WEBSITE

Yangting Lin: http://sourcedb.igg.cas.cn/cn/zjrck/200907/t20090713_2065532.html
Chunlai Li: https://people.ucas.ac.cn/~lichunlai?language=en
Xian-Hua Li: http://sourcedb.igg.cas.cn/cn/zjrck/200907/t20090713_2065535.html